TIS7 and SKMc15 Regulate Adipocyte Differentiation and Intestinal Lipid Absorption

[1]Ilja Vietor*, [1,13]Domagoj Cikes, [1,14]Kati Piironen, [1,15]Ronald Gstir, [2]Ivan Tancevski, [2,16]Philipp Eller, [2]Egon Demetz, [3]Michael Hess, [4]Volker Kuhn (†), [5]Gerald Degenhart, [6]Johannes Rainer, [7,8]Jan Rozman, [9,10,11]Martin Klingenspor, [7,8,12]Martin Hrabe de Angelis, [1]Taras Valovka, [1]Lukas A. Huber

[1]Division of Cell Biology, Biocenter, [2]Department of Internal Medicine II, [3]Department of Histology, [4]Department Trauma Surgery, [5]Department Radiology, Medical University Innsbruck, Austria, [6]Institute for Biomedicine, Eurac Research, Bolzano, Italy, [7]German Mouse Clinic, Institute of Experimental Genetics, Helmholtz Zentrum München, German Research Center for Environmental Health, Neuherberg, Germany, [8]German Center for Diabetes Research (DZD), Neuherberg, Germany, [9]Chair of Molecular Nutritional Medicine, Technical University of Munich, School of Life Sciences, Weihenstephan, Freising, Germany, [10]EKFZ - Else Kröner Fresenius Center for Nutritional Medicine, Technical University of Munich, Freising, Germany, [11]ZIEL - Institute for Food & Health, Technical University of Munich, Freising, Germany, [12]Chair of Experimental Genetics, Technical University of Munich, School of Life Sciences, Weihenstephan, Freising, Germany, [13]IMBA, Institute of Molecular Biotechnology of the Austrian Academy of Sciences, Vienna, Austria, [14]Division of Pharmaceutical Chemistry and Technology, Faculty of Pharmacy, University of Helsinki, Finland, [15]ADSI – Austrian Drug Screening Institute GmbH, Innsbruck, Austria, [16]Department of Internal Medicine, Medical University Graz, Austria

* Address correspondence to: Ilja Vietor, Division of Cell Biology, Biocenter, Innsbruck Medical University, Innrain 80-82, A-6020 Innsbruck, Austria. Phone: +43 512 9003 70175 E-mail: ilja.vietor@i-med.ac.at

† Deceased May 2019

Conflict of interest: The authors have declared that no conflict of interest exists.

Abstract

Adipogenesis is a complex process governed by multiple signaling cascades operating through various regulatory factors and specific downstream genes. Here we identified TIS7 (IFRD1) and its orthologue SKMc15 (IFRD2) as new regulators of adipogenesis and fat metabolism. Mice deficient in both TIS7 and SKMc15 (dKO) had severely reduced adipose tissue and were resistant to diet-induced obesity. Wnt signaling, a negative regulator of adipocyte differentiation, was significantly up regulated in TIS7 SKMc15 dKO mice. Elevated levels of the Wnt/β-catenin target protein Dlk-1 inhibited the expression of adipogenesis regulators PPARγ and C/EBPα, and fatty acid transporter CD36. Although both, TIS7 and SKMc15, contributed to this phenotype, TIS7 acted by controlling Wnt signaling and SKMc15 utilized a distinct mechanism. Our study suggests that TIS7 and SKMc15 play an important role in the control of lipid uptake and contribute to the regulation of adipocyte differentiation.

Nonstandard abbreviations used: CD36, cluster of differentiation 36; HFD, high fat diet; IFRD, interferon related developmental regulator; RD, regular diet; SKMc15, skeletal muscle cDNA library clone15; TIS7, TPA Induced Sequence 7

Introduction

Novel approaches for treating obesity-related conditions depend on the understanding of adipogenesis as a complex process in which multipotent stem cells are converted to preadipocytes before terminal differentiation into adipocytes [1]. The mechanisms that promote preadipocyte commitment and maturation involve protein factor regulators, epigenetic factors, and miRNAs. Detailed characterization of this process is therefore currently an area of intense research. TPA Induced Sequence 7 (TIS7) protein has been shown to be involved in the mainly transcriptional regulation of differentiation processes in various cell types, e.g. neurons [2, 3], enterocytes [4], myocytes [5, 6] and also adipocytes [7].

Multiple lines of evidence link the regulation of Wnt/β-catenin signaling to the physiological function of TIS7 [8], known in human as Interferon related developmental regulator 1 (IFRD1) [7,9,10]. TIS7 deficiency leads to a significant up regulation of Wnt/β-catenin transcriptional activity in both primary osteoblasts and in mouse embryonic fibroblasts (MEFs) derived from TIS7 knockout mice [9,10]. Recent data show that TIS7 is also involved in the control of adipocytes differentiation in mice [7]. TIS7 was found to be up regulated in both visceral (vWAT) and subcutaneous (sWAT) white adipose tissues (WAT) of genetically obese ob/ob mice [7]. TIS7 transgenic mice have increased total body adiposity and decreased lean mass compared with normal littermates [4]. On HFD, TIS7 transgenic mice exhibit a more rapid and proportionately greater gain in body weight with persistently elevated total body adiposity [4]. Enhanced triglyceride (TG) absorption in the gut of TIS7 transgenic mice [4] indicated that TIS7 expressed in the gut epithelium has direct effects on fat absorption in enterocytes. On the other hand, we have shown that as a result of impaired intestinal lipid absorption TIS7 knockout mice displayed lower body adiposity [11]. Compared with wild type (WT) littermates, TIS7 knockout mice do not gain weight when chronically fed a HFD and TIS7 deletion results in delayed lipid absorption and altered intestinal and hepatic lipid trafficking, with reduced intestinal TG, cholesterol, and free fatty acid mucosal levels in the jejunum [11,12]. However, at this point, the precise mechanism of TIS7 action in the regulation of lipid absorption and metabolism on the molecular level was unclear. TIS7 protein functions as a transcriptional co-regulator [13] due to its interaction with protein complexes containing either histone deacetylases (HDAC) [6,9,14-16] or protein methyl transferases, in particular PRMT5 [17]. The analysis of the adipocyte differentiation in preadipocytic 3T3-L1 cells suggested the involvement of TIS7 in the regulation of adipogenesis in the Wnt/β-catenin signaling context [7].

SKMc15, also known as Interferon related developmental regulator 2 (IFRD2), a second member of TIS7 gene family, is highly conserved in different species [18]. Mouse TIS7 and SKMc15 are highly homologous, with a remarkable identity at both the cDNA and amino acid levels (58% and 88%, respectively). However, there is so far no information about the physiological function and mechanisms of action of SKMc15 and its possible involvement in differentiation of various tissues remains to be studied.

Adipogenesis occurs late in embryonic development and in postnatal periods. Adipogenic transcription factors CCAAT/enhancer binding protein α (C/EBPα) and peroxisome proliferator activated receptor γ (PPARγ) play critical roles in adipogenesis and in the induction of adipocyte markers [19-20]. PPARγ is the major downstream target of Delta-like protein 1 (DLK-1). It is turned off by the induction of the MEK/ERK pathway leading to its phosphorylation and

proteolytic degradation [21]. DLK-1, also known as Pref-1 (preadipocyte factor 1) activates the MEK/ERK pathway to inhibit adipocyte differentiation [22]. C/EBPα that is highly expressed in mature adipocytes [23] can bind DNA and together with PPARγ to a variety of respective target genes [23]. Besides that, PPARγ binding to C/EBPα induces its transcription, thereby creating a positive feedback loop [24]. These two proteins have synergistic effects on the differentiation of adipocytes that requires a balanced expression of both C/EBPα and PPARγ [23].

One of the extracellular signaling pathways known to specifically affect adipogenesis is the Wnt/β-catenin signaling pathway [25-29]. Wnt signaling maintains preadipocytes in an undifferentiated state through inhibition of C/EBPα and PPARγ [20,30,31]. PPAR-γ and Wnt/β-catenin pathways are regarded as master mediators of adipogenesis [32]. Wnt signaling is a progenitor fate determinator and negatively regulates preadipocyte proliferation through DLK-1 [33-35]. Mice over-expressing DLK-1 are resistant to HFD-induced obesity, whereas DLK-1 knockout mice have accelerated adiposity [33]. DLK-1 transgenic mice show reduced expression of genes controlling lipid import (CD36) and synthesis (Srebp1c, Pparγ) [36]. The DLK-1 expression coincides with an altered recruitment of the protein methyl transferase 5 (PRMT5) and β-catenin to the DLK-1 promoter [37]. PRMT5 acts as a co-activator of adipogenic gene expression and differentiation [38]. SRY (sex determining region Y)-box 9 (Sox9), a transcription factor expressed in preadipocytes, is down regulated preceding adipocyte differentiation [39]. DLK-1 prevents down regulation of Sox9 by activating ERK, resulting in inhibition of adipogenesis [39]. The PRMT5- and histone-associated protein COPR5, affects PRMT5 functions related to cell differentiation [40]. Adipogenic conversion is delayed in MEFs derived from COPR5 KO mice [37] and WAT of COPR5 knockout mice is reduced when compared to control mice. DLK-1 expression is up regulated in COPR5 knockout cells [37].

Here we show for the first time that TIS7 and SKMc15, two members of a gene family, regulate not only intestinal lipid absorption, but mainly the process of adipocyte differentiation. TIS7 SKMc15 double knockout (dKO) mice had strongly decreased amounts of the body fat when fed with even regular, chow diet. We found two independent molecular mechanisms through which TIS7 and SKMc15 fulfill this function in a synergistic manner. TIS7 regulates the Wnt signaling pathway activity and thereby restricts DLK-1 protein levels allowing adipocyte differentiation. In contrast to that, SKMc15 knockout did not affect Wnt signaling. Importantly, dKO mice displayed a dominantly leaner phenotype when compared to TIS7 single knockout mice. The ablation of both TIS7 and SKMc15 genes was accompanied by a decrease in genes essential for adipocyte differentiation and function. Since TIS7 SKMc15 dKO mice render a substantially leaner phenotype on chow diet, without any challenge by HFD-induction, we propose that TIS7 and SKMc15 represent novel players in the process of physiological adipocyte differentiation and fat uptake in the intestines.

Results

Mice lacking TIS7 and SKMc15 genes have lower body mass, less fat and are resistant against HFD-induced obesity.
To identify a potential role of the TIS7 orthologous protein SKMc15 in pathophysiological processes, we generated SKMc15 KO mice (Supplementary figure 1). These mice were viable and fertile, but significantly ($p<0.001$) smaller than their WT littermates (body mass; Supplementary figure 2a) and mainly, as determined by Dual Energy X-ray Absorptiometry (DEXA), they had reduced fat mass (Supplementary figure 2b). On the contrary, the total body mass of TIS7 single KO mice was slightly (-5.1 %), but not significantly lower than the WT. In order to clarify whether both, TIS7 and SKMc15 are involved in the regulation of the adipocyte differentiation and/or the fat metabolism and if they act through same or different mechanisms, we have generated mice lacking both TIS7 and SKMc15 genes by crossing TIS7 with SKMc15 single KO mice. Double heterozygous mice were mated and the pups were genotyped by PCR. The genotype of the analyzed pups corresponded to the predicted Mendelian distribution. However, the number of pups born per litter was significantly lower ($P<0.01$) when compared to their WT littermates (Supplementary figure 2c). dKO pups were viable, and adult male and female mice were fertile. At birth the body weight of dKO and WT littermate mice were similar. Nevertheless, already during the weaning period, both the male and female dKO mice failed to gain weight when compared to their WT littermates. The reduced body weight gain persisted in the following weeks when the mice were fed regular diet (RD; chow diet) containing 11 % kcal of fat (Figure 1a). At 10 weeks of age, both male and female dKO mice displayed 30 % and later up to 44.9 % lower body weight compared with WT mice. Thus, ablation of TIS7 and SKMc15 genes resulted in strong reduction of body weight of mice kept on regular diet. These data suggested that TIS7 and SKMc15 do not play a role in the growth regulation during the prenatal development, but most probably affect postnatal fat uptake and/or adipocyte differentiation.

DEXA was performed to assess the total body fat content of dKO mice. 6-month-old WT mice had substantially higher amounts of fat than their dKO littermates, i.e. the percentage of fat was in the WT mice 37.7 ± 4 % vs. 6 ± 3 % of the total body mass in dKO animals. Furthermore, the percentage of lean tissue mass in WT animals was lower than in dKO animals (60 ± 4.6 % vs. 92 ± 3.14 %; Figure 1b). Next, we have analyzed the contribution of TIS7 and SKMc15 to the whole-body fat content of mice. 3-dimensional reconstitution images based on micro-computed tomography (micro-CT) technology disclosed that both TIS7 and SKMc15 KO mice had less abdominal fat than WT controls and mainly that the double knockout of both TIS7 and SKMc15 genes caused the strongest decrease in both, abdominal fat content and size (Figure 1c). The quantitative analyses of micro-CT analyses confirmed previous measurements showing that TIS7 deficiency caused a substantial lack of the abdominal fat tissues ($P=0.002$ when compared to WT mice). Whereas TIS7 knockout mice had less fat mass but were not significantly smaller ($P=0.068$) than their WT littermates, SKMc15 knockout were smaller ($P=0.007$) and leaner ($P=0.0001$) and dKO mice were highly significantly smaller ($P = 0.0001$) and had significantly less abdominal fat ($P=0.006$) than the WT mice (Figure 1d).

Given the differences in body weight and adiposity we conducted an indirect calorimetry (IC) trial monitoring over 21 hours gas exchange (oxygen consumption and carbon dioxide production), activity (distance and rearing), and food intake with sex- and age-matched WT and dKO animals. We measured body mass before and after the trial and determined rectal body temperature. Food intake and energy expenditure were analyzed using a linear model including

body mass as a covariate. Rectal body temperature determined after the IC trial did not differ (36.56 WT and 36.71 dKO mice). The typical daily pattern of oxygen consumption during the IC trial was observed in WT and dKO mice. Mean oxygen consumption correlated with the different body masses of WT and dKO mice. Maximal oxygen consumption (VO_2) values were lower in the dKO mice (81.12 ml/l vs. 107.28 in WT mice). However, when adjusted to the body mass difference, they corresponded well to the reduced body mass. Using this approach, no genotype effect on oxygen consumption could be detected. There was also no substantial genotype effect on food intake, although when adjusted to the body mass this was non-significantly increased in dKO mice (4.0 g WT and 3.4 g dKO mice). Apart from minor differences observed during the first hours of the trial, respiratory exchange ratios (RER = VCO_2/VO_2) were identical in WT and dKO mice (Supplementary figure 3a). Concerning the activity, no effects could be detected in the total travelled distance (928 cm/20 min WT and 874 cm/20 min dKO mice) and rearing behavior (116 rearing/20 min WT and 96 rearing/20 min dKO mice). In summary, in TIS7 SKMc15 dKO mice we have identified substantially reduced body weight, mainly because of lacking fat. These differences were found despite the identical food intake, activity and no major differences in several metabolic parameters.

To investigate potential links between TIS7, SKMc15 and obesity, we studied the response of dKO mice to HFD. At 2 months of age, male mice were housed individually and fed with HFD for 21 days. Food intake was measured every second day and body weight was measured every fourth day. Feces were collected every second day to analyze the composition of excreted lipids and blood samples were collected after the third week of HFD feeding to measure the concentrations of hepatic and lipoprotein lipases, respectively. Already within the first week of HFD feeding, WT mice gained more weight than the dKO mice (Figure 1e), although there were no obvious differences in food consumption (Supplementary figure 3c) or in levels of lipolytic enzymes (Supplementary figures 3d, e). These differences in body weight gain continued to increase during the second and third week, at which time the body weight of WT mice increased additionally for 30% (30.0 ± 2.3%) when compared with the beginning of the HFD feeding period. In contrast, the weight of dKO animals increased only slightly (7.6 ± 1.6%) (Figure 1e and Supplementary figure 2d). Both genes, TIS7 and SKMc15 contributed to this phenotype and we could see an additive effect following their deletion (Figure 1e).

TIS7 and SKMc15 are required for efficient intestinal lipid absorption, dKO mice have increased serum TG and decreased serum glucose levels.

Previous studies showed that intestinal over-expression of TIS7 caused increased intestinal lipid transport resulting in elevated body weight gain during HFD feeding [41]. To test the hypothesis that TIS7 and SKMc15 dKO impaired absorption of free fatty acids from the lumen into enterocytes we administered olive oil by oral gavages to HFD-fed WT and dKO mice. After one-week adaptation to HFD, there was lower TGs accumulation in the intestines of dKO mice (3 hours after bolus oil feeding) as detected by oil red O staining (Figure 2a). To examine the kinetics of dietary fat entry into the serum, mice were orally given [^{3}H]-triolein. Radioactivity levels in plasma samples from dKO mice were rising markedly slower than those of WT mice (Figure 2b), confirming a reduced rate of fat absorption from intestines into the circulation. Interestingly, while fed with HFD, dKO mice had higher concentrations of free fatty acids in the feces (109 ± 10.4 µmol/g) when compared to the WT animals (78 ± 6.5 µmol/g) (Figure 2c) and a consequent increase in feces

energy content (WT: 14.442 ± 0.433 kJ/g dry mass compared to dKO: 15.497 ± 0.482 kJ/g dry mass, Figure 2d). Thus, lack of TIS7 and SKMc15 reduced efficient free fatty acid uptake in the intestines of mice. Unexpectedly, dKO mice had increased postprandial serum TG levels (Figure 2e). Furthermore, 4 hours after intragastric administration of olive oil dKO mice displayed an inability to clear TGs from the circulation (Supplementary figure 3b). There was also a reduction of postprandial serum glucose levels in dKO mice (Figure 2f), which remained up to 10 hours of the fasting period. Therefore, we investigated WT and dKO mice in an intraperitoneal glucose tolerance test. In contrast to WT mice, dKO mice had an increased ability to deal with a glucose load indicating an increased rate of blood glucose clearance (Figure 2g). Although our experiments suggested that dKO mice suffer from an intestinal lipid uptake deficiency, yet another contributing reason for the lean phenotype of dKO mice may be that TIS7 and SKMc15 regulate the adipocyte differentiation.

Adipocyte differentiation in TIS7 SKMc15 dKO mice is inhibited due to up regulated Wnt signaling and DLK-1 secretion regulated via β-catenin.

Primary MEFs derived from totipotent cells of early mouse mammalian embryos are capable of differentiating into adipocytes and they are versatile models to study adipogenesis as well as mechanisms related to obesity such as genes, transcription factors and signaling pathways implicated in the adipogenesis process [42]. To test whether TIS7 and SKMc15 are required for adipogenesis we treated MEFs derived from WT, SKMc15 and TIS7 single and dKO mice, using an established adipocyte differentiation protocol [41]. Eight days after initiation of adipocyte differentiation a remarkable reduction of adipocyte differentiation potential in SKMc15, TIS7 KO MEFs and dKO MEFs was observed, as characterized by the formation of lipid droplets stained by oil red O (Figure 3a). Quantification of this staining revealed that fat vacuole formation in cells derived from SKMc15, TIS7 and dKO mice represented 65 %, 35 % and 24 % of the WT cells, respectively (Figure 3b). These data indicated that both, TIS7 and SKMc15 were also equally critical for adipocyte differentiation. Furthermore, these results suggested that the defect in adipogenesis could be responsible for the resistance of dKO mice to HFD-induced obesity.

Wnt/β-catenin signaling is an important regulatory pathway for adipocyte differentiation [43,28]. Consistently, others and we have shown that TIS7 deficiency causes up regulation of Wnt/β-catenin transcriptional activity [9,10]. Therefore, we have assessed Wnt signaling activity in MEFs by measuring transcriptional activity with TOPflash luciferase reporter assays. As shown in Figure 3c, Wnt signaling activity, when compared to the WT MEFs, was not regulated in SKMc15 KO, but significantly up regulated in TIS7 KO (8-fold increase; $P<0.0001$) and dKO MEFs (2-fold increase; $P<0.01$). Next, we analyzed total β-catenin levels by Western blotting in 3 biological replicates of WAT from WT and dKO mice. WAT of dKO showed 2 fold up regulation of β-catenin protein levels (Figure 3d) when compared to WT mice (Figure 3d). This suggested that TIS7 and SKMc15 may also affect levels of Wnt signaling target genes. Therefore, we further analyzed the expression of DLK-1, a negative regulator of adipogenesis and known target of Wnt signaling [37,44]. The qPCR analysis showed a significant up regulation of DLK-1 mRNA levels in both dKO WAT ($P<0.01$) and MEFs ($P<0.05$) when compared to the WT (Figure 3e). Moreover, whereas in the WT MEFs the expression of DLK-1 was strongly up regulated only during the first day of adipocyte differentiation, in dKO MEFs, treated with the same adipocyte differentiation cocktail, DLK-1 was up regulated ($P<0.001$) throughout the entire 8 days of the differentiation (Figure

3f). This result was confirmed on the protein level by Western blot analyses of lysates from 8 day differentiated adipocytes (Figure 3g). A rescue experiment was conducted to confirm that the regulation of DLK-1 expression was TIS7- and SKMc15-dependent. dKO MEFs were transiently transfected with TIS7, SKMc15 or combination of TIS7 and SKMc15 vectors and 48 hours later the mRNA expressions were analyzed by RT qPCR. The ectopic expression of TIS7 down regulated the DLK-1 expression more significantly ($P<0.01$) than the over-expression of SKMc15 ($P<0.05$) or as the co-expression of TIS7 and SKMc15 ($P<0.05$) (Figure 3h). Based on these data we concluded that TIS7 and SKMc15 are required to restrain the DLK-1 levels, most probably through the Wnt/β-catenin signaling pathway.

DLK-1 protein has a protease cleavage site in its extracellular domain [45] and is secreted. Hence, adding soluble DLK-1 to the medium inhibits adipogenesis [44]. To test if the dKO MEFs secreted DLK-1, cell culture media from MEFs treated 8 days with the adipocyte differentiation cocktail were collected and analyzed by Western blotting. As shown in figure 3i, dKO secreted DLK-1 protein, but in an identical volume of the cell culture medium from WT MEFs no DLK-1 could be detected. To prove that secreted DLK-1 could inhibit adipocyte differentiation of dKO MEFs, we cultured WT MEFs with conditioned medium from dKO MEFs. Adipocyte differentiation of WT MEFs was strongly inhibited by the dKO MEFs-conditioned medium when compared to the control WT cells (Figure 3j). Based on these results we concluded that tissues of TIS7 SKMc15 dKO mice and cells derived from those express increased DLK-1 levels and secreted, soluble DLK-1 may inhibit adipocyte differentiation *in vivo*.

According to the data presented above, TIS7 and/or SKMc15 are involved in the regulation of DLK-1 expression. Since the molecular requirements for this regulation were so far unresolved we proceeded with chromatin immunoprecipitation (ChIP) experiments, where we studied the binding of known and novel transcription factors to the DLK-1 regulatory region. Our earlier study showed that TIS7 directly binds to DNA and also regulates gene expression via PRMT5 [17]. Therefore, we tested in DLK-1 ChIP experiments the direct binding of both TIS7 and SKMc15, as well as symmetrically dimethylated histones H4 and β-catenin, proteins involved in the transcriptional regulation of DLK-1 [37]. We found increased β-catenin binding ($P<0.0001$) and reduced amounts of histone H4, symmetrically dimethylated at the arginine 3 residue at the DLK-1 regulatory element in dKO, but not in WT MEFs treated 8 days with the adipocyte differentiation cocktail (Figure 3k). However, neither in WT nor in dKO MEFs we could identify any direct binding of TIS7 or SKMc15 proteins to the DLK-1 regulatory elements. These results suggested that TIS7 and SKMc15 epigenetically regulate DLK-1 expression indirectly, i.e. affecting β-catenin levels and its binding to the DLK-1 regulatory region, rather than *via* their direct binding to DLK-1 regulatory elements.

TIS7 and SKMc15 regulate adipocyte differentiation through DLK-1, MEK/ERK pathway and adipogenic regulators PPARγ and C/EBPα.

Previous studies showed that soluble DLK-1 activates MEK/ERK signaling, which is required for inhibition of adipogenesis [22]. As DLK-1 was strongly up regulated in dKO MEFs during adipocyte differentiation we subsequently analyzed possible activation of the MEK/ERK pathway manifested by increased phosphorylation of proteins p42 and p44. The activation of MEK/ERK was up regulated in dKO adipocyte-differentiated MEFs (Figure 4a). The phosphorylation of p44 and of p42 was up regulated 5-fold and 3-fold ($P<0.05$), respectively in the adipocyte-differentiated dKO when compared to the WT MEFs (Figure 4b). Previously, activation of MEK/ERK by DLK-1 was

shown to up regulate the expression of the transcription factor SOX9, resulting in the inhibition of adipogenesis [39]. Therefore, we measured SOX9 mRNA expression by RT qPCR in 8 days adipocyte-differentiated MEFs. SOX9 expression was highly significantly ($P<0.001$) up regulated in 8 days adipocyte-differentiated dKO when compared to WT MEFs (Figure 4c).

The adipocyte differentiation deficiency of dKO MEFs suggested that C/EBPα and PPARγ might also be regulated through TIS7 and/or SKMc15. It was previously shown that DLK-1 activates the MEK/ERK pathway [22] and furthermore that elevated levels of the cleaved ectodomain of DLK1 have been correlated with reduced expression of PPARγ [46,47]. Therefore, we analyzed the differences in PPARγ expression between WT and dKO MEFs during their differentiation into adipocytes. As long as PPARγ expression was strongly induced during WT MEFs adipocyte differentiation this was barely detectable in dKO MEFs (Figure 4d). Also C/EBPα expression in TIS7/SKMc15 dKO MEFs stayed low and was never induced up to the levels of WT (Figure 4e). In a rescue experiment we showed that the co-expression of TIS7 and SKMc15 strongly increased the expression of the PPARγ in dKO MEFs ($P<0.001$), almost up to the levels of WT MEFs (Figure 4f). The expression of yet another adipogenic regulator C/EBPα was also strongly up regulated by the co-expression of TIS7 and SKMc15 ($P<0.01$) (Figure 4g). Based on these results we concluded that TIS7 and SKMc15 regulate the expression of both PPARγ and C/EBPα, two master regulator genes crucial for the adipocyte differentiation.

TIS7 and SKMc15 regulate the expression of the lipid transporters CD36 and DGAT1.

To determine whether decreased intestinal lipid absorption might be caused by changes in expression of lipid processing and transporting molecules, we performed transcriptome analyses of total RNA samples isolated from the small intestines of HFD-fed WT type and dKO animals. Cluster analyses of lipid transport-related gene transcripts revealed differences between WT type and dKO animals in the expression of adipogenesis regulators, such as peroxisome proliferator-activated receptors γ (PPARγ) and δ [48], fatty acid binding proteins 1 and 2 (FABP1, 2) [49], cytoplasmic fatty acid chaperones expressed in adipocytes, acyl-coenzyme A synthetases 1 and 4 (ACSL1,4) found to be associated with histone acetylation in adipocytes, lipid loading and insulin sensitivity [50], SLC27a1, a2 fatty acid transport proteins, critical mediators of fatty acid metabolism [51], angiotensin-converting enzyme (ACE) playing a regulatory role in adipogenesis and insulin resistance [52], CROT, a carnitine acyltransferase important for the oxidation of fatty acids, a critical step in their metabolism [53], phospholipase PLA2G5 robustly induced in adipocytes of obese mice [54-56]. Upon those, we decided to study in more detail the regulation of CD36 that encodes a very long chain fatty acids (VLCFA) transporter. The transmembrane protein CD36 is an important fatty acid transporter that facilitates a fatty acids (FA) uptake by heart, skeletal muscle, and also adipose tissues [57]. PPARγ induces CD36 expression in adipose tissue where it functions as a fatty acid transporter, and therefore, its regulation by PPARγ contributes to the control of blood lipids. Interestingly, CD36 null mice exhibit elevated circulating LCFA and triglycerides levels consistent with the phenotype of TIS7 SKMc15 dKO mice and CD36 deficiency partially protected from HFD-induced insulin resistance [57-59]. Using three different probe sets we identified a statistically significant down regulation of CD36 gene expression in the jejunum of dKO mice (2.1-, 2-, and 2.7-fold down regulation) (Figure 5a bottom). Reduced CD36

mRNA and protein levels in small intestines of dKO mice were independently confirmed in a larger cohort of animals (n=8; Figure 5b). Immunohistochemical staining of CD36 in small intestines of HFD-fed mice showed a down regulation in the number of CD36-positive cells, as well as an in the signal intensity in enterocytes of dKO mice when compared to WT (Figure 5c). These data correlated well with changes identified in CD36 mRNA and protein levels (Figure 5b). Since CD36 is expressed in the adipose tissues [60] we analyzed its expression in the WAT of WT and dKO mice. CD36 mRNA expression was strongly reduced in WAT from dKO mice (64 % of the WT values) (Figure 5d). Next, we analyzed CD36 in WT and dKO MEFs before the onset and during the adipocyte differentiation. As long as CD36 mRNA expression during the eight days of differentiation substantially increased in WT MEFs, there were almost undetectable transcript levels of CD36 in dKO cells treated with the adipocyte differentiation cocktail (Figure 5e). Diacylglycerol acyltransferase 1 (DGAT1), a protein associated with the enterocytic triglyceride absorption and intracellular lipid processing [83] is besides CD36 another target gene of adipogenesis master regulator PPARγ [61]. DGAT1 mRNA levels are strongly up regulated during adipocyte differentiation [62], its promoter region contains a PPARγ binding site [91] and DGAT1 is also negatively regulated by the MEK/ERK pathway [92]. DGAT1 expression was shown to be increased in TIS7 transgenic mice [4] and its expression was decreased in the gut of high fat diet-fed TIS7 KO mice [11]. Importantly, DGAT1 expression in adipocytes and WAT is up regulated by PPARγ activation [61]. Therefore, we measured DGAT1mRNA levels during the differentiation of WT and TIS7 SKMc15 dKO MEFs into adipocytes to analyze the role of TIS7 and SKMc15 on the regulation of this protein involved in adipogenesis and triglyceride processing. As long as DGAT1 expression substantially increased during the differentiation of WT MEFs, there was no difference in DGAT1 mRNA levels in dKO cells treated with the adipocyte differentiation cocktail (Figure 5f). Based on these data we concluded that both, TIS7 and SKMc15 regulate expression of multiple proteins involved in fat uptake both in intestines and adipocytes thereby contributing to the lean phenotype of TIS7 SKMc15 dKO mice.

Discussion

In this study we show that simultaneous depletion of TIS7, a protein regulating cell differentiation [20,30,31] and of its orthologue SKMc15, a protein with until now unknown function caused in mice severe reduction of adipose tissues and resistance against high fat-induced obesity. We identified two parallel mechanisms leading to this strong phenotype. Firstly, it was the lack of fat adsorption in small intestines and secondly a deficiency in the adipocyte differentiation. As mechanisms leading to these two phenomena we pinpointed the TIS7-regulated Wnt signaling pathway and yet another SKMc15-dependent regulatory mechanism, both controlling in parallel the DLK-1 protein levels (Figure 6).

TIS7 SKMc15 dKO mice were phenotypically similar with both, CD36 deficient and DLK-1 transgenic mice, namely in decreased amounts of WAT and resistance to HFD-induced obesity. Based on previous studies with TIS7 single knockout mice we knew that TIS7 ablation leads to resistance against HFD-induced obesity [11,16], increases Wnt signaling pathway activity and regulates PRMT5 towards the regulatory regions of target genes [16,17]. Here we focused on the clarification of TIS7 and SKMc15 roles in the regulatory mechanisms of intestinal fat absorption and adipogenesis.

In TIS7 SKMc15 dKO mice we found inhibited PPARγ and C/EBPα levels, induced MEK/ERK pathway, and decreased expression of CD36 and DGAT1, all hallmarks of up regulated DLK-1. TIS7 and SKMc15 acted after the commitment to the preadipocyte stage since the elevated DLK-1 and β-catenin levels found in the white adipose tissue of TIS7 SKMc15 dKO mice are characteristic for the preadipocyte stage [44,63]. In addition, the lipid transport deficiency of intestinal enterocytes due to their lower CD36 expression levels also led to the impaired fat accumulation in TIS7 SKMc15 dKO mice. The lack of intestinal CD36 caused higher secretion of free fatty acids, important building blocks of TG synthesis and also of fat accumulation in target tissues.

TIS7 SKMc15 dKO mice helped us to understand the biological functions and potential synergisms of TIS7 and SKMc15 activities *in vivo*. During adipocyte differentiation of WT MEFs we have identified differential expression patterns for TIS7 and SKMc15. While TIS7 mRNA levels reached maximum values on day 3 of the adipocyte differentiation and its expression increased 6-fold when compared to the MEFs, SKMc15 reached expression plateau on day 5 and was 2.5-fold increased. These data suggested that both proteins play a regulatory role in adipogenesis, however differ in their mechanisms and timing. To further support this statement, our data show that TIS7 knockout strongly up regulated Wnt signaling whereas SKMc15 knockout had no effect. The disruption of Wnt signaling in embryonic fibroblasts results in spontaneous adipocyte differentiation [29,64] and opposite, stabilized β-catenin keeps cells in the preadipocyte stage [29]. Consistent with this we found up regulated β-catenin protein levels in WAT of TIS7 SKMc15 dKO mice and increased Wnt signaling activity in TIS7 SKMc15 dKO MEFs. We demonstrated that increase in Wnt signaling lead to up regulated β-catenin binding to the DLK-1 gene regulatory elements resulting in sustained DLK-1 expression in TIS7 SKMc15 dKO MEFs induced for adipocyte differentiation. In the adipogenesis is DLK-1 expression down regulated through histone methylation by COPR5 and PRMT5 that prevent β-catenin binding to the DLK-1 gene [37]. Interestingly, we found that symmetric dimethylation of H4R3 at the DLK-1 promoter was reduced in dKO MEFs consistent with our previous findings on the role of TIS7 in epigenetic regulation [17]. There was a difference in effects of ectopic expression of TIS7, SKMc15 and their co-expression on DLK-1 levels, suggesting that TIS7 and

SKMc15 might be involved in two independent pathways/mechanisms of DLK-1 transcriptional regulation. Despite the fact that SKMc15 knockout had no effect on Wnt signaling it also affected DLK-1 mRNA levels suggesting a contribution of SKMc15 to transcriptional regulation of this gene. Recently SKMc15 (IFRD2) was identified as a novel factor capable to translationally inactivate ribosomes [65]. Since down regulation of the protein synthesis machinery is essential regulatory event during early adipogenic differentiation [66], it is possible that SKMc15 may also regulate DLK-1 protein levels through translational regulation, however additional investigations will be necessary. Elevated DLK-1 levels in TIS7 SKMc15 dKO MEFs activated the MEK/ERK pathway thereby decreasing PPARγ and C/EBPα levels important for adipogenic differentiation. Besides that, the expression of SOX9 was up regulated [22], suggesting that the TIS7 SKMc15 dKO MEFs keep their proliferative state and cannot enter differentiation into mature adipocytes [22].

Down regulation of PPARγ and C/EBPα implied changes in expression of downstream adipogenesis-related genes. Among them, decreased CD36 and DGAT1 levels were a plausible explanation of the dKO mice lean phenotype since it is known that both proteins play a functional role in differentiation of murine adipocytes and their deficiency impairs fat pad formation independent of lipid uptake [67]. On the other hand, reduced CD36 expression might explain higher fecal free fatty acid concentrations and elevated serum TG levels due to reduced free fatty acid uptake in multiple cell types of TIS7 SKMc15 dKO mice. Moreover, CD36-deficient mice have phenotypical characteristics (resistance to HFD-induced obesity [68]; impaired intestinal lipid uptake [69]; higher plasma triglyceride levels, and lower plasma glucose levels [70]) that are almost identical to our TIS7 SKMc15 dKO mice. Our findings implicate that TIS7 and SKMc15 play a role in the regulation of CD36 and therefore possibly contribute to CD36 related pathogenesis of human metabolic diseases, such as hypoglycemia [71], hypertriglyceridemia [72], and disordered fatty acid metabolism [73-75].

TIS7 SKMc15 dKO mice had under both, chow and HFD conditions decreased body weight. Comparing dKO with single knockout mice we showed that both TIS7 and SKMc15 contributed to this phenotype in a synergistic manner. We also identified similar synergism of TIS7 and SKMc15 knockout effects on the body fat content. Our data presented here explain the phenotype on the molecular level and propose that TIS7 and SKMc15 regulated both, fat absorption in the small intestine and adipocytes differentiation. Because of high similarity between TIS7 and SKMc15 genes with their human IFRD1 and IFRD2 homologues our findings may be relevant for the treatment of obesity and related metabolic disorders.

Methods

Animal maintenance and experimental procedures. Animals were maintained in the same room on a 12:12-hour light/dark photoperiod at an ambient temperature of 22 ± 2 °C. At the end of the experiment, animals were killed by cervical dislocation. All animal experiments were performed in accordance with the Austrian Tierversuchsgesetz (in accordance with Austrian legislation BGB1 Nr. 501/1988 i.d.F. 162/2005) and have been granted by the Bundesministerium für Bildung, Wissenschaft und Kultur.

Generation of animal models. Mice lacking TIS7 were generated as previously described [6]. SKMc15 knockout mice were generated as following: The targeting construct contained all 12 exons of the SKMc15 gene locus. A loxP site and a neomycin resistance gene (neomycin cassette) were inserted into intron 1 at position 105515 (AY162905). The neomycin cassette was flanked by two frt sites. A second loxP site was inserted after the poly A tail into the 3´ UTR of the SKMc15 gene at position 102082 (AY162905). Further downstream, 15 additional nucleotides, part of intron 1, exon 2 (splice site: donor and acceptor) and the CDS of hrGFP from the Vitality hrGFP mammalian expression vector pIRES-hrGFP-2a (Stratagene) with its poly A tail were added next to the loxP site. The targeted construct was electroporated into Sv129 mouse embryonic stem (ES) cells. After the selection with G418 single cell clones were expanded and screened by PCR. Positive PCR results were confirmed by Southern blot analysis. Cre deletion was performed by adding Cre recombinase (encoded by the phage P1) to the cell culture medium. After the recombinase treatment cell clones (the sequence from exon 2 to exon 12 and the frt site flanked the neomycin cassette were designed to be specifically removed) were screened by PCR for the deleted allele. The cre recombinase-mediated deletion resulted into a gene product consisting of the SKMc15 WT promoter, exon 1, intron 1 (with inserted loxP site), 9 nucleotides of the exon 2, and additional 14 nucleotides for in-frame link to the hrGFP coding sequence. The hrGFP coding sequence was followed by 442 bp poly A tail and the SKMc15 wt locus continuing at the position 102078 (AY162905). PCR results were confirmed by Southern blot analysis. Clones in which the floxed gene part was successfully deleted, were used for blastocyst injection into C57Bl/6J recipient mice. We received two male chimeras for the deleted construct with ≥ 40 % or more agouti coat color. These chimeras were mated to C57Bl6 females for germ-line transmission. There was one case of successful germline transmission. Thus, the knockout mouse strain was derived from only one male mouse carrying the allele of interest. Heterozygous mice were more back-crossed to C57Bl6 mice to reduce the Sv129 genome fraction and after 9 generations mice were assumed to have a clean C57Bl6 background. TIS7 SKMc15 dKO mice were generated by crossing the SKMc15 knockout mice with the TIS7 single knockout mice [6]. The resulting mice were screened by PCR and double heterozygous mice used for further breeding until homozygosity.

SKMc15 knockout Southern blot analysis. Three XbaI restriction sites (upstream of exon 1, position 109042; adjacent to the poly A tail, position 102079; and about 10 kb downstream of the poly A tail, position 92253) are located in the SKMc15 locus (AY162905). Due to the insertion of the loxP site followed by the hrGFP cassette the restriction site 2 was lost. The fragment detected by the Southern probe, was 9.6 kb in the wt (Supplementary figure 1a, insert, band V) and 15 kb in the deleted locus (band IV). The 566 bp long probe for hybridization was synthesized by PCR from

genomic DNA (positions 96605 – 97171; AY162905). PCR primer sequences for the probe synthesis were: RK 150 Fwd: 5'- GGTCCTGCCACTAATGCACTG-3'; RK 151 Rev: 5'- GCAGACAGATGCCAGGAAGAC-3'.

SKMc15 knockout PCR genotyping analysis. The hrGFP insert in the 3´ UTR was detected by the forward primer (GFP2) located in the GFP cassette (5´¬AGCCATACCACATTTGTAGAG-3´) and the reverse primer (RK101) in the 3´ UTR (5´-TGATGATAGCTTCAAAGAGAA- 3´; position 100617 – 100591 of the SKMc15 locus (AY162905). The resulting PCR product was 1700 bp long. For SKMc15 detection were used forward (RG1; 5´-TGTGGCCTTTATCCTGAGTC-3´; position 102286 – 102266) and reverse (RG2; 5´-TGGCTTCATTTACACTACTCCTT-3´; position 101860 – 101882) primers flanking the hrGFP insert of the targeted locus (Supplementary figure 1a). The WT allele PCR product was 426 bp and the targeted allele PCR product was 1772 bp long (Supplementary figure 1b). The SKMc15 deleted allele lacked the binding site for RG1 and therefore did not give any product. The genotype of TIS7 was tested as explained previously [6] and shown in supplementary figure 1c.

Growth monitoring and body composition measurement. To monitor long-term growth, mice were weaned at 3 weeks of age onto the regular chow diet (RD), and weighed weekly. Body composition of RD-fed 24 weeks old mice was analyzed by dual energy X-ray absorptiometry (DEXA) with a Norland scanner (Fisher Biomedical). White and brown adipose tissue was isolated from 1-year-old TIS7 SKMc15 dKO and WT male mice for histochemical analysis.
Micro-computed tomography (micro-CT) experiments were performed using a vivaCT 40 (Scanco Medical AG, Brüttisellen, Switzerland). The scans were performed using 250 projections with 1024 samples, resulting in a 38µm isotropic resolution. The tube settings were 45kV voltage, 177µA current and an integration time of 300ms per projection. The acquired images have a matrix of 1024*1024 voxels and a grayscale depth of 16 bit. The length of the image stack is individually dependent, starting from the cranial end of the fist lumbar vertebrae, to the caudal end of the fifth lumbar vertebrae. The image reconstruction and post processing was performed using the system workstation of the micro-CT. For the adipose tissue evaluation a IPL (image processing language, Scanco Medical AG) script published by Judex et al., provided by Scanco medical AG was modified to the scanner individual parameters, leading to a slightly differing threshold (2 values lower thresholds than in the original script) for the adipose tissue filters [76]. The script calculates the total abdominal volume without potential air in the cavities, the visceral adipose tissue volume and the subcutaneous adipose tissue volume. For quantitative comparison the percent contribution of the abdominal fat to the body weight was calculated, using a mean weight of 0.9196 g/ml for adipose tissue [77]. Statistics were performed using an ANOVA with a Bonferroni corrected Post Hoc testing on the µCT fat data and the body mass data.

Metabolic measurements. The indirect calorimetry trial monitoring gas exchange (oxygen consumption and carbon dioxide production), activity (distance and rearing), and food intake was conducted over a period of 21 hours (PhenoMaster TSE Systems GmbH, Bad Homburg, Germany). Body mass before and after the trial was measured and rectal body temperature (approximately at 10 AM, before transfer of mice back to their home cages, was

measured). The genotype effects were statistically analyzed using 1 way ANOVA. Food intake and energy expenditure were analyzed using a linear model including body mass as a co-variate.

HFD feeding. Age-matched (7-10 week old) male TIS7-/- SKMc15-/-mice and WT controls were caged individually and maintained from 3 weeks up to 8 weeks on a synthetic, high saturated fat (HFD) diet (TD.88137; Ssniff); 42% kcal from milk fat, 0.2% kcal from cholesterol). Animals were weighted every 4th day between 08:00 and 10:00. Small intestines were harvested for oil red O staining to detect lipid accumulation. Intestines, liver, muscles and adipose tissue were collected for total RNA and protein isolation. Unfixed intestines were flushed with PBS using a syringe, embedded in Tissue-Tek (Sakura, 4583) and frozen in liquid nitrogen for immunohistochemical analysis.
Quantitative food consumption and fecal fat determination. For monitoring food intake and weight gain, adult mice were acclimatized to individual caging and to the HFD for a week, monitored for weight gain and their food intake daily. The daily food intake data were pooled for the following 7 days and the food intake was estimated (g/day). Feces were collected daily and weighted for 7 days after second week of the HFD consumption. 50 mg of dried feces were boiled in 1 ml alkaline methanol (1M NaOH/Methanol, 1 3 v/v) at 80°C for 2 h after addition of 50 nmol 5α-Cholestane (Sigma, C8003) as internal standard for neutral sterol analysis. After cooling down to room temperature, neutral sterols were extracted using three times 3 ml of petroleum ether, boiling range 60–80°C. The residual sample was diluted 1:9 with distilled water. 100 µl of the solution were subjected to an enzymatic total bile acid measurement. The extracted neutral sterols were converted to trimethylsilyl derivatives. Neutral sterol composition of prepared feces samples was determined by capillary gas chromatography on an Agilent gas chromatograph (HP 6890) equipped with a 25 m×0.25 mm CP-Sil-19 fused silica column (Varian) and a Flame Ionization Detector. The working conditions were the following: Injector temperature 280°C; pressure 16.0 psi; column flow constant at 0.8 ml/min; oven temperature program: 240°C (4 min), 10°C/min to 280°C (27 min); detector temperature 300°C [78]. Energy content of dried egested feces samples (~ 1 g per sample) was determined by bomb calorimetry (IKA C 7000, IKA, Staufen, Germany) [79].

Biochemical assays. Plasma triglycerides concentrations were measured employing the Chol2 COBAS (03039773190) commercial kit (Roche). Blood glucose levels were measured using the One Touch Ultra 2 device (LifeScan Inc.). Hepatic and lipoprotein lipase concentrations were measured as previously described [80]. Blood samples were always collected in the morning after 4 hours fasting. For glucose tolerance test, mice were given an intraperitoneal injection of 2 g/kg glucose, and blood glucose was subsequently measured at the indicated time points.

In vivo intestinal triglyceride absorption analysis. TIS7 SKMc15 dKO mice and WT littermates maintained on a RD were food-deprived for 4 h. Mice received a bolus (60 microliters per body weight through intragastric gavages) of olive oil, then they were sacrificed at indicated time points and intestines harvested to detect lipid accumulation using toluidine blue staining. The same experiment was repeated with animals fed with HFD for one week and their intestines were stained with oil red O. For quantitative studies, a bolus of 200 µl olive oil (Carapelli) containing 1 mCi (9,10-3H(N9))-triolein (Perkin Elmer, NET431001MC) was orally administered to mice using an infusion cannula with a bulb end (Acufirm Ernst Kratz). Blood samples were collected 0, 1, and 2 h after the oral gavage for scintillation counter

measurement of the absorbed serum 3H-triolein amount. To inhibit the clearance of plasma triacylglycerol, 100 µl of the surfactant tyloxapol (5% in PBS, Sigma-Aldrich, T8761) were administered through intraperitoneal injection [81].

Antibodies, viral and cDNA constructs. Antibodies used for immunofluorescence and Western blot analysis of CD36 were purchased from AbD Serotec (MCA2748) and Abcam (ab36977) respectively. p44/42 MAPK (Erk1/2) and Phospho-p44/42 MAPK (Erk1/2) (Thr202/Tyr204) antibodies were from Cell Signaling Technology (9102, 9101), rabbit anti-β-catenin antibody was from Sigma (C2206) and mouse monoclonal anti-DLK antibody from Abcam (ab119930). anti-Histone H4R3me2s antibody used for chromatin immunoprecipitation was purchased from Active Motif (61187). For CD36 promoter activity assay, we used PGLCD36 construct kindly provided by Dr. Paul Shore (University of Manchester, UK). Luciferase reporter construct pTOPflash was a gift from Prof. H. Clevers (University of Utrecht, Holland). TIS7 construct used for luciferase assays was described previously [14] Partial cds of mSKMc15 was amplified by PCR and cloned into pcDNA3.1(-)/MycHis6 (Invitrogen). For CD36 rescue experiment, we used CD36 over-expressing Adenovirus (Ad-CD36) that was kindly provided by Dr. Jason Dyck [82].

Histochemical and immunohistochemical analyses. Tissues were fixed in Bouine fixative, dehydrated through increasing concentrations of ethanol, cleared and embedded in paraffin, sectioned and stained with hematoxylin and eosin (H&E) or toluidine blue. To demonstrate intracellular tissue lipids, formalin-fixed (3.7% v/v) tissue was cryoprotected with sucrose (30% v/v) and frozen sections were stained with oil red O. Immunofluorescence was performed using anti-mouse CD36 (dilution 1:100) as primary antibodies and incubated at 4°C overnight. Alexa Fluor 488–conjugated goat anti-rabbit IgG (Invitrogen, A-11034) was used as secondary antibody and incubated at room temperature for 1 hour. As a negative control, secondary antibody was used without prior incubation of sections with a primary antibody.

Cell culture and adipocyte differentiation. MEFs were generated from 16 day old embryos obtained from WT and dKO pregnant female mice. Briefly, after dissection of head for genotyping, and removal of limbs, liver and visceral organs in order to prevent the contamination with other types of cells, embryos were minced and incubated in 1 mg/mL collagenase (Sigma-Aldrich, C2674) for 30 minutes at 37°C. Embryonic fibroblasts were then plated and before adipocyte differentiation experiments maintained in growth medium containing: Dulbecco's modified Eagle medium (DMEM), high glucose (4.5 g/l); sodium pyruvate, L-glutamine, 10% fetal calf serum (FCS) (Invitrogen, 41966029), 10% penicillin/streptomycin at 37°C in an atmosphere of 5% CO2. For adipocyte differentiation, 2-day-postconfluent cells (day 0) were treated with growth medium supplemented with: 0.5 mM 3-isobutyl-1-methylxanthine (I5879), 1 µM dexamethasone (D4902), 5 µg/ml insulin (I2643) and 1 µM Rosiglitazone (Sigma-Aldrich, R2408). After 3 days, medium was switched to growth medium containing only 1 µg/ml insulin and cells were differentiated for 8 days. On day 8, were adipocytes stained with oil red O to visualize lipid accumulation. Briefly, cells were washed with phosphate-buffered saline (PBS), fixed with 6 % formaldehyde solution overnight, washed with ddH_2O twice, incubated 5 minutes with 60 % isopropanol, air dried and then incubated 10 min at RT with oil red O working solution and washed 4 times

with ddH_2O. Microscopic analysis was done at this point. Afterwards was oil red O stain eluted with 100 % isopropanol and the absorbance was measured at 490 nm.

RNA collection for microarray analysis and quantitative RT-PCR. Tissues from animals fed for 3 weeks with HFD were snap frozen and stored at –80°C. Total RNA was isolated using the TRIzol reagent (Invitrogen, 15596026). RNA was then chloroform-extracted and precipitated with isopropanol. The yield and purity of RNA was determined by spectroscopic analysis; RNA was stored at –80°C until use.

RNA microarray analysis. Gene expression profiling analysis was performed by the Expression Profiling Unit at the Innsbruck Medical University according to the following protocol. For total RNA isolation, a combination of TRIreagent (MRC Inc., TR 118) and RNAeasy spin columns (Quiagene, 4380204) was used according to the manufacturers' protocols. RNA quantity and purity was determined by optical density measurements (OD260/280) and RNA integrity by using the 2100 Bioanalyzer (Agilent Technologies). Only high quality RNA was further processed. For Affymetrix GeneChip analysis 500 ng total RNA was processed to generate a biotinylated hybridization target using "One Cycle cDNA Synthesis" and "One Cycle Target Labelling" kits from Affymetrix (A10752030) according to the manufacturer's protocols. In brief, total RNA was reverse-transcribed into cDNA using an anchored oligo-dTT7-Primer, converted into double-stranded cDNA and purified with the "Affymetrix Sample Clean-up Kit". Thereafter, cRNA was generated by T7 polymerase-mediated in vitro transcription including a modified nucleotide for subsequent biotinylation. Following RNA purification, 20 µg of cRNA were fragmented at 95° using the Affymetrix fragmentation buffer, mixed with hybridization buffer containing hybridization controls and hybridized to the GeneChips (Mouse Genome 430 2.0). The arrays were stained and washed in an Affymetrix fluidic station 450. Fluorescence signals were recorded by an Affymetrix scanner 3000 and image analysis performed with the GCOS software. All further analyses were performed in R (http://www.r-project.org) using packages from the Bioconductor project (version 2.6) [83]. Functions from the affyPLM package were used for quality assessments of the microarrays and only good quality arrays were further analysed. GeneChip raw expression values were normalized and summarized using the GCRMA method [84]. p-values for significance of differential expression were calculated using the moderated t test [85] and adjusted for multiple hypothesis testing using the method from Benjamini and Hochberg [86]. Genes with an adjusted p-value < 0.05 were considered significantly differentially expressed. Microarray raw and pre-processed data has been deposited to Gene Expression Omnibus, accession number GSE27019.

Quantitative RT-PCR and statistics. 5 µg total RNA obtained from tissues, were treated with DNAse1 and reverse transcribed to cDNA by Revert Aid First Strand cDNA Synthesis Kit (Thermo Fisher Scientific, K1622) with oligo dT primers. Quantitative RT-PCR was performed using Taqman probes and primer sets (Applied Biosystems) specific for CD36 (assay ID Mm00432398_m1), Dgat1 (Mm00515643_m1), Pparγ (Mm00440940_m1), C/EBPα (Mm00514283_s1), DLK-1 (Mm00494477_m1) and Sox9 (Mm00448840_m1). A probe and primer set for ribosomal protein 20 (assay ID Mm02342828_g1) were used as normalization control allowing quantification by the comparative

ddCt method. PCR reactions were performed by using 10 µl cDNA per reaction in PikoReal 96 real-time PCR system (Thermo Scientific). Quantification data were analyzed by 2-tailed, type 2 Student's t test.

Transient transfections and luciferase assay. pGL2-Basic (Promega, E1641) or pGLCD36 (Shore, 2002 #4139) were used as reporter constructs. Expression constructs or empty vector DNA used as a control were co-transfected. pCMV-β-Gal plasmid expressing β-galactosidase protein was used to normalize for transfection efficiency. Full length TIS7 cDNAs was described before [14]. For luciferase reporter assays, 1.5x105 cells were seeded into 24-well plates and transfected after 24 hours with indicated plasmid combinations using Lipofectamine Plus™ Reagent (Invitrogen, 15338030). The total amount of transfected DNA (2 µg DNA per well) was equalized by addition of empty vector DNA. Cells were harvested 48 h post-transfection in 0.25 M Tris, pH 7.5, 1% Triton X-100 buffer and assayed for both luciferase and β-galactosidase activities. Luciferase activity and β-galactosidase activity (as a control for transfection efficiency) were assayed in parallel by using the Lucy 2® detection system (Anthos). All luciferase values were corrected for transfection efficiency by the corresponding β-galactosidase values. Transfections were performed in triplicates and all experiments were repeated several times.

Primary muscle cell culture, protein extraction and Western blot analysis. Adult primary MSC cultures of WT and dKO mice were prepared as previously described [6]. For protein extraction, proteins from MSCs were harvested using Mammalian Cell Lysis Kit (Sigma-Aldrich, MCL1-1KT) according to the manufacturer's protocol. For Western blot analysis, 30 µg of the cell extracts were resolved by 12.5% SDS-PAGE under reducing conditions and transferred onto polyvinylidene difluoride membranes (Sigma-Aldrich, IPFL00005). The membranes were incubated with blocking buffer (5% milk in PBS) to block non-specific reaction and then exposed to the mouse anti-CD36 antibodies (1:500) overnight at 4°C. After washing 3 times with PBS containing 2% Tween-20 (Sigma-Aldrich, P1379), membranes were incubated with peroxidase-conjugated anti-rabbit IgG (Sigma-Aldrich, A0545). Specificity of the antibody was tested incubating part of the membrane with the blocking peptide (1 µg/mL; Abcam, ab66772). Chemiluminescence reagents (Supersignal West Pico Chemiluminescence substrate; Thermo Scientific, 34577) were used to visualize the labeled protein bands according to the manufacturer's instructions. The membranes were then incubated with stripping buffer (0.1 M NaOH, 0.5 M NaCl) and examined with tubulin antibodies (Sigma-Aldrich, SAB4500087), respectively. Each experiment was performed three times and representative blots are shown.

In vitro free fatty acid uptake and viral infection. Micelles were generated as recently described [69] by drying down under N2 0.38 mg of 1-palmitoyl-2-oleoyl-sn-glycero-3-phosphocholine (POPC, Sigma-Aldrich, 26853-31-6), 0.02 mg of cholesterol (Sigma-Aldrich, C8667), and trace amounts of 3H¬lipids. Samples were resuspended in 10 ml of PBS containing 5 mM taurocholate (TCA, pH 7.4, Sigma-Aldrich, 345909-26-4) with gentle rocking at ambient temperature. The following radiolabeled 3H-labeled fatty acids were used: palmitic acid (16:0) and lignoceric acid (24:0) (American Radiolabeled Chemicals, ART 1986, ART 0865). MSCs were plated into 24-well culture dishes; at 80% confluence they were washed twice with PBS (ambient temperature) and incubated with 400 microlitres of lipid micelles containing 100,000 dpm of the indicated 3H- labeled lipids for 3 min. The cells were then washed three times with PBS and

dissolved in 0.1mM NaOH. The associated radioactivity was determined by liquid scintillation counting. Data are expressed as the fractional uptake (the percentage of the total radioactivity applied to the cells which remains cell-associated following three washes with PBS).

Chromatin immunoprecipitation (ChIP). Chromatin was isolated from TIS7 WT and dKO formaldehyde-treated MEFs using the EpiSeeker Chromatin Extraction Kit (Abcam, ab117152) according to the manufacturer protocol. ChIP analyses were carried out as described previously [87]. In brief, sonicated chromatin was centrifuged at 15.000x g for 10 min at 4°C, and the supernatant (65 µg of sheared DNA per each IP) was diluted ten-fold with cold ChIP dilution buffer containing 16.7 mM Tris-HCl pH 8.1, 167 mM NaCl, 0.01% (w/v) SDS, 1.1% (w/v) Triton X-100 and 1.2 mM EDTA supplemented with protease inhibitors. Diluted chromatin samples were pre-cleared for 1 h with 55µl of 50% suspension of protein A sepharose (Protein A Sepharose CL-4B, Sigma-Aldrich, 17-0780-01) beads that were blocked with 0.2 µg/µl sonicated herring sperm DNA (Thermo Fisher, 15634017) and 0.5 µg/µl BSA (NEB, B9000 S). Immunoprecipitations were performed using 4 µg of antibodies at 4°C overnight. Immune complexes were collected with 75 µl of 50% suspension of protein A Sepharose for 1h at 4°C followed by centrifugation at 1000 rpm and 4°C for 5 min. using table top centrifuge. The beads carrying the immune complexes were washed once with 1ml low salt wash buffer (20 mM Tris-HCl pH 8.1, 150 mM NaCl, 0.1%(w/v) SDS, 1%(w/v) Triton X-100 (Merck), 2 mM EDTA), once with high salt wash buffer (20 mM Tris-HCl pH 8.1, 500 mM NaCl, 0.1% (w/v) SDS, 1% (w/v) Triton X-100, 2 mM EDTA), once with LiCl wash buffer (10 mM Tris-HCl pH 8.1, 250 mM LiCl, 1% (w/v) sodium deoxycholate, 1% (w/v) IGEPAL-CA630, 1 mM EDTA) for 5 min at 4°C on a rotating wheel, and finally twice with 1 ml TE buffer (10 mM Tris-HCl pH 8.0, 1 mM EDTA). Protein-DNA complexes were eluted from antibodies by adding a freshly prepared elution buffer containing 1% SDS and 0.1 M $NaHCO_3$. The eluate was reverse cross linked by adding 5M NaCl to a final concentration of 0.2 M and incubating at 65 °C for four hours. Afterwards the eluate was treated with Proteinase K at 45 °C for 1 hour. The immunoprecipitated DNA was then isolated by phenol/chloroform precipitation and used as a template for real-time-quantitative PCR. The primer pairs specific for regulatory regions of the Dlk-1 gene were selected as described before [37]. Reactions with rabbit IgG or with 1.23% of total chromatin (input) were used as controls. For real-time-quantitative PCR a PikoReal System was used. Signals were normalized to input chromatin and shown as % input. The raw cycle threshold (Ct) values of the input were adjusted to 100% by calculating raw Ct – log2(100/input). To calculate the % input of the immunoprecipitations, the equation 100 × 2[Ct (adjusted input to 100%) – Ct (IP)] was applied.

Statistics. Unpaired, 2-tailed Student's t tests were used for all statistical comparisons. A P value of < 0.05 was considered significant.

Acknowledgements

The authors especially thank Robert Kurzbauer from IMP Vienna for his participation in the generation of TIS7 SKMc15 dKO mice. We also acknowledge Angelika Floerl for the preparation of histological sections, Christiane Heim for serum analyses and free fatty acid uptake measurements, Frans Stellaard for the analysis of fatty acids content in feces,

Mayra Eduardoff for RNA processing for Affymetrix chip analysis, Laura M. de Smalen and Karin Schluifer for the technical assistance, David Teis and Zlatko Trajanoski for the critical reading of the manuscript. Furthermore, we would like to thank Dr. Paul Shore for providing us with the pGLCD36 construct. We are indebted to the staff at the Animal Facility of Innsbruck Medical University for their care of our mice. This work was supported by P18531-B12 and P22350-B12 grants from the Austrian FWF grant agency to Ilja Vietor and by the German Federal Ministry of Education and Research (Infrafrontier grant 01KX1012) to Martin Hrabe de Angelis.

Contributions

I.V., D.C., I.T., V.K., J.Ra., J.Ro., M.K., T.V. and L.A.H. designed the study. I.V., D.C., K.P., R.G., P.E., E.D., J.Ra., J.Ro., M.H., V.K., G.D., F.S., and T.V. performed experiments. I.V., D.C., T.V. and L.A.H. wrote the manuscript.

References

1 Sarantopoulos, C. N. *et al.* Elucidating the Preadipocyte and Its Role in Adipocyte Formation: a Comprehensive Review. *Stem Cell Rev* **14**, 27-42, doi:10.1007/s12015-017-9774-9 (2018).

2 Arenander, A. T. *et al.* TIS gene expression in cultured rat astrocytes: induction by mitogens and stellation agents. *J Neurosci Res* **23**, 247-256 (1989).

3 Iacopetti, P., Barsacchi, G., Tirone, F. & Cremisi, F. Expression of the PC4 gene in the developing rat nervous system. *Brain Res* **707**, 293-297. (1996).

4 Wang, Y. *et al.* Targeted intestinal overexpression of the immediate early gene tis7 in transgenic mice increases triglyceride absorption and adiposity. *J Biol Chem* **280**, 34764-34775 (2005).

5 Guardavaccaro, D., Ciotti, M. T., Schafer, B. W., Montagnoli, A. & Tirone, F. Inhibition of differentiation in myoblasts deprived of the interferon-related protein PC4. *Cell Growth.Differ.* **6**, 159-169 (1995).

6 Vadivelu, S. K. *et al.* Muscle regeneration and myogenic differentiation defects in mice lacking TIS7. *Mol Cell Biol* **24**, 3514-3525 (2004).

7 Nakamura, Y. *et al.* Repression of adipogenesis through promotion of Wnt/beta-catenin signaling by TIS7 up-regulated in adipocytes under hypoxia. *Biochim Biophys Acta* **1832**, 1117-1128, doi:10.1016/j.bbadis.2013.03.010 (2013).

8 Arenander, A. T. *et al.* TIS gene expression in cultured rat astrocytes: multiple pathways of induction by mitogens. *J Neurosci Res* **23**, 257-265 (1989).

9 Vietor, I., Kurzbauer, R., Brosch, G. & Huber, L. A. TIS7 regulation of the beta-catenin/Tcf-4 target gene osteopontin (OPN) is histone deacetylase-dependent. *J Biol Chem* **280**, 39795-39801 (2005).

10 Iezaki, T. *et al.* The Transcriptional Modulator Interferon-Related Developmental Regulator 1 in Osteoblasts Suppresses Bone Formation and Promotes Bone Resorption. *J Bone Miner Res* **31**, 573-584, doi:10.1002/jbmr.2720 (2016).

11 Yu, C. *et al.* Deletion of Tis7 protects mice from high-fat diet-induced weight gain and blunts the intestinal adaptive response postresection. *J Nutr* **140**, 1907-1914, doi:10.3945/jn.110.127084 (2010).

12 Garcia, A. M. *et al.* Tis7 deletion reduces survival and induces intestinal anastomotic inflammation and obstruction in high-fat diet-fed mice with short bowel syndrome. *Am J Physiol Gastrointest Liver Physiol* **307**, G642-654, doi:10.1152/ajpgi.00374.2013 (2014).

13 Micheli, L. *et al.* PC4 Coactivates MyoD by Relieving the Histone Deacetylase 4-Mediated Inhibition of Myocyte Enhancer Factor 2C. *Mol Cell Biol* **25**, 2242-2259 (2005).

14 Vietor, I. *et al.* TIS7 interacts with the mammalian SIN3 histone deacetylase complex in epithelial cells. *Embo J* **21**, 4621-4631 (2002).

15 Wick, N., Schleiffer, A., Huber, L. A. & Vietor, I. Inhibitory effect of TIS7 on Sp1-C/EBPalpha transcription factor module activity. *J Mol Biol* **336**, 589-595 (2004).

16 Park, G. *et al.* The transcriptional modulator Ifrd1 controls PGC-1alpha expression under short-term adrenergic stimulation in brown adipocytes. *The FEBS journal* **284**, 784-795, doi:10.1111/febs.14019 (2017).

17 Lammirato, A. *et al.* TIS7 induces transcriptional cascade of methylosome components required for muscle differentiation. *BMC Biol* **14**, 95, doi:10.1186/s12915-016-0318-6 (2016).

18 Latif, F. *et al.* The human homolog of the rodent immediate early response genes, PC4 and TIS7, resides in the lung cancer tumor suppressor gene region on chromosome 3p21. *Hum Genet* **99**, 334-341. (1997).

19 Farmer, S. R. Transcriptional control of adipocyte formation. *Cell Metab* **4**, 263-273, doi:10.1016/j.cmet.2006.07.001 (2006).

20 Rosen, E. D. & MacDougald, O. A. Adipocyte differentiation from the inside out. *Nat Rev Mol Cell Biol* **7**, 885-896, doi:10.1038/nrm2066 (2006).

21 Wang, Y. & Sul, H. S. Pref-1 regulates mesenchymal cell commitment and differentiation through Sox9. *Cell Metab* **9**, 287-302, doi:10.1016/j.cmet.2009.01.013 (2009).

22 Kim, K. A., Kim, J. H., Wang, Y. & Sul, H. S. Pref-1 (preadipocyte factor 1) activates the MEK/extracellular signal-regulated kinase pathway to inhibit adipocyte differentiation. *Mol Cell Biol* **27**, 2294-2308, doi:10.1128/MCB.02207-06 (2007).

23 Lefterova, M. I. *et al.* PPARgamma and C/EBP factors orchestrate adipocyte biology via adjacent binding on a genome-wide scale. *Genes Dev* **22**, 2941-2952, doi:10.1101/gad.1709008 (2008).

24 Lowell, B. B. PPARgamma: an essential regulator of adipogenesis and modulator of fat cell function. *Cell* **99**, 239-242 (1999).

25 van Tienen, F. H., Laeremans, H., van der Kallen, C. J. & Smeets, H. J. Wnt5b stimulates adipogenesis by activating PPARgamma, and inhibiting the beta-catenin dependent Wnt signaling pathway together with Wnt5a. *Biochem Biophys Res Commun* **387**, 207-211, doi:10.1016/j.bbrc.2009.07.004 (2009).

26 Li, H. X., Luo, X., Liu, R. X., Yang, Y. J. & Yang, G. S. Roles of Wnt/beta-catenin signaling in adipogenic differentiation potential of adipose-derived mesenchymal stem cells. *Mol Cell Endocrinol* **291**, 116-124, doi:10.1016/j.mce.2008.05.005 (2008).

27 Nishizuka, M., Koyanagi, A., Osada, S. & Imagawa, M. Wnt4 and Wnt5a promote adipocyte differentiation. *FEBS Lett* **582**, 3201-3205, doi:10.1016/j.febslet.2008.08.011 (2008).

28 Kennell, J. A. & MacDougald, O. A. Wnt signaling inhibits adipogenesis through beta-catenin-dependent and -independent mechanisms. *J Biol Chem* **280**, 24004-24010, doi:10.1074/jbc.M501080200 (2005).

29 Ross, S. E. *et al.* Inhibition of adipogenesis by Wnt signaling. *Science* **289**, 950-953 (2000).

30 MacDougald, O. A. & Lane, M. D. Transcriptional regulation of gene expression during adipocyte differentiation. *Annu Rev Biochem* **64**, 345-373, doi:10.1146/annurev.bi.64.070195.002021 (1995).

31 Tontonoz, P. & Spiegelman, B. M. Fat and beyond: the diverse biology of PPARgamma. *Annu Rev Biochem* **77**, 289-312, doi:10.1146/annurev.biochem.77.061307.091829 (2008).

32 Xu, C. *et al.* Cross-Talking Between PPAR and WNT Signaling and its Regulation in Mesenchymal Stem Cell Differentiation. *Curr Stem Cell Res Ther* **11**, 247-254 (2016).

33 Moon, Y. S. *et al.* Mice lacking paternally expressed Pref-1/Dlk1 display growth retardation and accelerated adiposity. *Mol Cell Biol* **22**, 5585-5592 (2002).

34 Mortensen, S. B. *et al.* Membrane-tethered delta-like 1 homolog (DLK1) restricts adipose tissue size by inhibiting preadipocyte proliferation. *Diabetes* **61**, 2814-2822, doi:10.2337/db12-0176 (2012).

35 Smas, C. M. & Sul, H. S. Pref-1, a protein containing EGF-like repeats, inhibits adipocyte differentiation. *Cell* **73**, 725-734 (1993).

36 Barclay, J. L. *et al.* GH-dependent STAT5 signaling plays an important role in hepatic lipid metabolism. *Endocrinology* **152**, 181-192, doi:10.1210/en.2010-0537 (2011).

37 Paul, C., Sardet, C. & Fabbrizio, E. The Wnt-target gene Dlk-1 is regulated by the Prmt5-associated factor Copr5 during adipogenic conversion. *Biol Open* **4**, 312-316, doi:10.1242/bio.201411247 (2015).

38 LeBlanc, S. E. *et al.* Protein arginine methyltransferase 5 (Prmt5) promotes gene expression of peroxisome proliferator-activated receptor gamma2 (PPARgamma2) and its target genes during adipogenesis. *Mol Endocrinol* **26**, 583-597, doi:10.1210/me.2011-1162 (2012).

39 Sul, H. S. Minireview: Pref-1: role in adipogenesis and mesenchymal cell fate. *Mol Endocrinol* **23**, 1717-1725, doi:10.1210/me.2009-0160 (2009).

40 Paul, C., Sardet, C. & Fabbrizio, E. The histone- and PRMT5-associated protein COPR5 is required for myogenic differentiation. *Cell Death Differ* **19**, 900-908, doi:10.1038/cdd.2011.193 (2012).

41 Wang, S. *et al.* Wnt1 positively regulates CD36 expression via TCF4 and PPAR-gamma in macrophages. *Cell Physiol Biochem* **35**, 1289-1302, doi:10.1159/000373951 (2015).

42 Ruiz-Ojeda, F. J., Ruperez, A. I., Gomez-Llorente, C., Gil, A. & Aguilera, C. M. Cell Models and Their Application for Studying Adipogenic Differentiation in Relation to Obesity: A Review. *Int J Mol Sci* **17**, doi:10.3390/ijms17071040 (2016).

43 Prestwich, T. C. & Macdougald, O. A. Wnt/beta-catenin signaling in adipogenesis and metabolism. *Curr Opin Cell Biol* **19**, 612-617, doi:10.1016/j.ceb.2007.09.014 (2007).

44 Garces, C., Ruiz-Hidalgo, M. J., Bonvini, E., Goldstein, J. & Laborda, J. Adipocyte differentiation is modulated by secreted delta-like (dlk) variants and requires the expression of membrane-associated dlk. *Differentiation* **64**, 103-114, doi:10.1046/j.1432-0436.1999.6420103.x (1999).

45 Lee, Y. L., Helman, L., Hoffman, T. & Laborda, J. dlk, pG2 and Pref-1 mRNAs encode similar proteins belonging to the EGF-like superfamily. Identification of polymorphic variants of this RNA. *Biochim Biophys Acta* **1261**, 223-232 (1995).

46 Smas, C. M., Chen, L. & Sul, H. S. Cleavage of membrane-associated pref-1 generates a soluble inhibitor of adipocyte differentiation. *Mol Cell Biol* **17**, 977-988, doi:10.1128/mcb.17.2.977 (1997).

47 Lee, K. *et al.* Inhibition of adipogenesis and development of glucose intolerance by soluble preadipocyte factor-1 (Pref-1). *J Clin Invest* **111**, 453-461, doi:10.1172/JCI15924 (2003).

48 Lefterova, M. I., Haakonsson, A. K., Lazar, M. A. & Mandrup, S. PPARgamma and the global map of adipogenesis and beyond. *Trends Endocrinol Metab* **25**, 293-302, doi:10.1016/j.tem.2014.04.001 (2014).

49 Garin-Shkolnik, T., Rudich, A., Hotamisligil, G. S. & Rubinstein, M. FABP4 attenuates PPARgamma and adipogenesis and is inversely correlated with PPARgamma in adipose tissues. *Diabetes* **63**, 900-911, doi:10.2337/db13-0436 (2014).

50 Joseph, R. *et al.* ACSL1 Is Associated With Fetal Programming of Insulin Sensitivity and Cellular Lipid Content. *Mol Endocrinol* **29**, 909-920, doi:10.1210/me.2015-1020 (2015).

51 Anderson, C. M. & Stahl, A. SLC27 fatty acid transport proteins. *Mol Aspects Med* **34**, 516-528, doi:10.1016/j.mam.2012.07.010 (2013).

52 Riedel, J., Badewien-Rentzsch, B., Kohn, B., Hoeke, L. & Einspanier, R. Characterization of key genes of the renin-angiotensin system in mature feline adipocytes and during in vitro adipogenesis. *J Anim Physiol Anim Nutr (Berl)* **100**, 1139-1148, doi:10.1111/jpn.12392 (2016).

53 Zhou, S. *et al.* Increased missense mutation burden of Fatty Acid metabolism related genes in nunavik inuit population. *PLoS One* **10**, e0128255, doi:10.1371/journal.pone.0128255 (2015).

54 Pettersson, C. *et al.* Increased lipolysis by secretory phospholipase A(2) group V of lipoproteins in diabetic dyslipidaemia. *J Intern Med* **264**, 155-165, doi:10.1111/j.1365-2796.2008.01932.x (2008).

55 Wootton, P. T. *et al.* Tagging SNP haplotype analysis of the secretory PLA2-V gene, PLA2G5, shows strong association with LDL and oxLDL levels, suggesting functional distinction from sPLA2-IIA: results from the UDACS study. *Hum Mol Genet* **16**, 1437-1444, doi:10.1093/hmg/ddm094 (2007).

56 Sergouniotis, P. I. *et al.* Biallelic mutations in PLA2G5, encoding group V phospholipase A2, cause benign fleck retina. *Am J Hum Genet* **89**, 782-791, doi:10.1016/j.ajhg.2011.11.004 (2011).

57 Coburn, C. T. *et al.* Defective uptake and utilization of long chain fatty acids in muscle and adipose tissues of CD36 knockout mice. *J Biol Chem* **275**, 32523-32529, doi:10.1074/jbc.M003826200 (2000).

58 Wilson, C. G. *et al.* Hepatocyte-Specific Disruption of CD36 Attenuates Fatty Liver and Improves Insulin Sensitivity in HFD-Fed Mice. *Endocrinology* **157**, 570-585, doi:10.1210/en.2015-1866 (2016).

59 Goudriaan, J. R. *et al.* CD36 deficiency increases insulin sensitivity in muscle, but induces insulin resistance in the liver in mice. *J Lipid Res* **44**, 2270-2277, doi:10.1194/jlr.M300143-JLR200 (2003).

60 Bonen, A. *et al.* FAT/CD36 expression is not ablated in spontaneously hypertensive rats. *J Lipid Res* **50**, 740-748, doi:10.1194/jlr.M800237-JLR200 (2009).

61 Koliwad, S. K. *et al.* DGAT1-dependent triacylglycerol storage by macrophages protects mice from diet-induced insulin resistance and inflammation. *J Clin Invest* **120**, 756-767, doi:10.1172/JCI36066 (2010).

62 Cases, S. *et al.* Identification of a gene encoding an acyl CoA:diacylglycerol acyltransferase, a key enzyme in triacylglycerol synthesis. *Proc Natl Acad Sci U S A* **95**, 13018-13023, doi:10.1073/pnas.95.22.13018 (1998).

63 Gautam, J. *et al.* Formononetin, an isoflavone, activates AMP-activated protein kinase/beta-catenin signalling to inhibit adipogenesis and rescues C57BL/6 mice from high-fat diet-induced obesity and bone loss. *Br J Nutr* **117**, 645-661, doi:10.1017/S0007114517000149 (2017).

64 Bennett, C. N., Hodge, C. L., MacDougald, O. A. & Schwartz, J. Role of Wnt10b and C/EBPalpha in spontaneous adipogenesis of 243 cells. *Biochem Biophys Res Commun* **302**, 12-16 (2003).

65 Brown, A., Baird, M. R., Yip, M. C., Murray, J. & Shao, S. Structures of translationally inactive mammalian ribosomes. *Elife* **7**, doi:10.7554/eLife.40486 (2018).

66 Marcon, B. H. *et al.* Downregulation of the protein synthesis machinery is a major regulatory event during early adipogenic differentiation of human adipose-derived stromal cells. *Stem Cell Res* **25**, 191-201, doi:10.1016/j.scr.2017.10.027 (2017).

67 Christiaens, V., Van Hul, M., Lijnen, H. R. & Scroyen, I. CD36 promotes adipocyte differentiation and adipogenesis. *Biochim Biophys Acta* **1820**, 949-956, doi:10.1016/j.bbagen.2012.04.001 (2012).

68 Hajri, T. *et al.* CD36-facilitated fatty acid uptake inhibits leptin production and signaling in adipose tissue. *Diabetes* **56**, 1872-1880, doi:10.2337/db06-1699 (2007).

69 Drover, V. A. *et al.* CD36 mediates both cellular uptake of very long chain fatty acids and their intestinal absorption in mice. *J Biol Chem* **283**, 13108-13115, doi:10.1074/jbc.M708086200 (2008).

70 Febbraio, M. A. & Dancey, J. Skeletal muscle energy metabolism during prolonged, fatiguing exercise. *J Appl Physiol (1985)* **87**, 2341-2347, doi:10.1152/jappl.1999.87.6.2341 (1999).

71 Nagasaka, H. *et al.* CD36 deficiency predisposing young children to fasting hypoglycemia. *Metabolism* **60**, 881-887, doi:10.1016/j.metabol.2010.08.008 (2011).

72 Kashiwagi, H. *et al.* Analyses of genetic abnormalities in type I CD36 deficiency in Japan: identification and cell biological characterization of two novel mutations that cause CD36 deficiency in man. *Hum Genet* **108**, 459-466 (2001).

73 Glazier, A. M., Scott, J. & Aitman, T. J. Molecular basis of the Cd36 chromosomal deletion underlying SHR defects in insulin action and fatty acid metabolism. *Mamm Genome* **13**, 108-113, doi:10.1007/s00335-001-2132-9 (2002).

74 Nozaki, S. *et al.* CD36 mediates long-chain fatty acid transport in human myocardium: complete myocardial accumulation defect of radiolabeled long-chain fatty acid analog in subjects with CD36 deficiency. *Mol Cell Biochem* **192**, 129-135 (1999).

75 Tanaka, T. *et al.* Defect in human myocardial long-chain fatty acid uptake is caused by FAT/CD36 mutations. *J Lipid Res* **42**, 751-759 (2001).

76 Lublinsky, S., Luu, Y. K., Rubin, C. T. & Judex, S. Automated separation of visceral and subcutaneous adiposity in in vivo microcomputed tomographies of mice. *J Digit Imaging* **22**, 222-231, doi:10.1007/s10278-008-9152-x (2009).

77 Neeland, I. J. *et al.* Associations of visceral and abdominal subcutaneous adipose tissue with markers of cardiac and metabolic risk in obese adults. *Obesity (Silver Spring)* **21**, E439-447, doi:10.1002/oby.20135 (2013).

78 Harchaoui, K. E. *et al.* Reduced fecal sterol excretion in subjects with familial hypoalphalipoproteinemia. *Atherosclerosis* **207**, 614-616, doi:10.1016/j.atherosclerosis.2009.06.022 (2009).

79 Pfluger, P. T. *et al.* Calcineurin Links Mitochondrial Elongation with Energy Metabolism. *Cell Metab* **22**, 838-850, doi:10.1016/j.cmet.2015.08.022 (2015).

80 Tancevski, I. *et al.* The thyromimetic T-0681 protects from atherosclerosis. *J Lipid Res* **50**, 938-944, doi:10.1194/jlr.M800553-JLR200 (2009).

81 Yen, C. L. *et al.* Deficiency of the intestinal enzyme acyl CoA:monoacylglycerol acyltransferase-2 protects mice from metabolic disorders induced by high-fat feeding. *Nat Med* **15**, 442-446, doi:10.1038/nm.1937 (2009).

82 Koonen, D. P. *et al.* Increased hepatic CD36 expression contributes to dyslipidemia associated with diet-induced obesity. *Diabetes* **56**, 2863-2871, doi:10.2337/db07-0907 (2007).

83 Gentleman, R. C. *et al.* Bioconductor: open software development for computational biology and bioinformatics. *Genome Biol* **5**, R80, doi:10.1186/gb-2004-5-10-r80 (2004).

84 Wu, Z. J., Irizarry, R. A., Gentleman, R., Martinez-Murillo, F. & Spencer, F. A model-based background adjustment for oligonucleotide expression arrays. *J Am Stat Assoc* **99**, 909-917, doi:10.1198/016214504000000683 (2004).

85 Smyth, G. K. Linear models and empirical bayes methods for assessing differential expression in microarray experiments. *Stat Appl Genet Mol Biol* **3**, Article3, doi:10.2202/1544-6115.1027 (2004).

86 Benjamini, Y., Drai, D., Elmer, G., Kafkafi, N. & Golani, I. Controlling the false discovery rate in behavior genetics research. *Behav Brain Res* **125**, 279-284 (2001).

87 Reintjes, A. *et al.* Asymmetric arginine dimethylation of RelA provides a repressive mark to modulate TNFalpha/NF-kappaB response. *Proc Natl Acad Sci U S A* **113**, 4326-4331, doi:10.1073/pnas.1522372113 (2016).

Figure 1

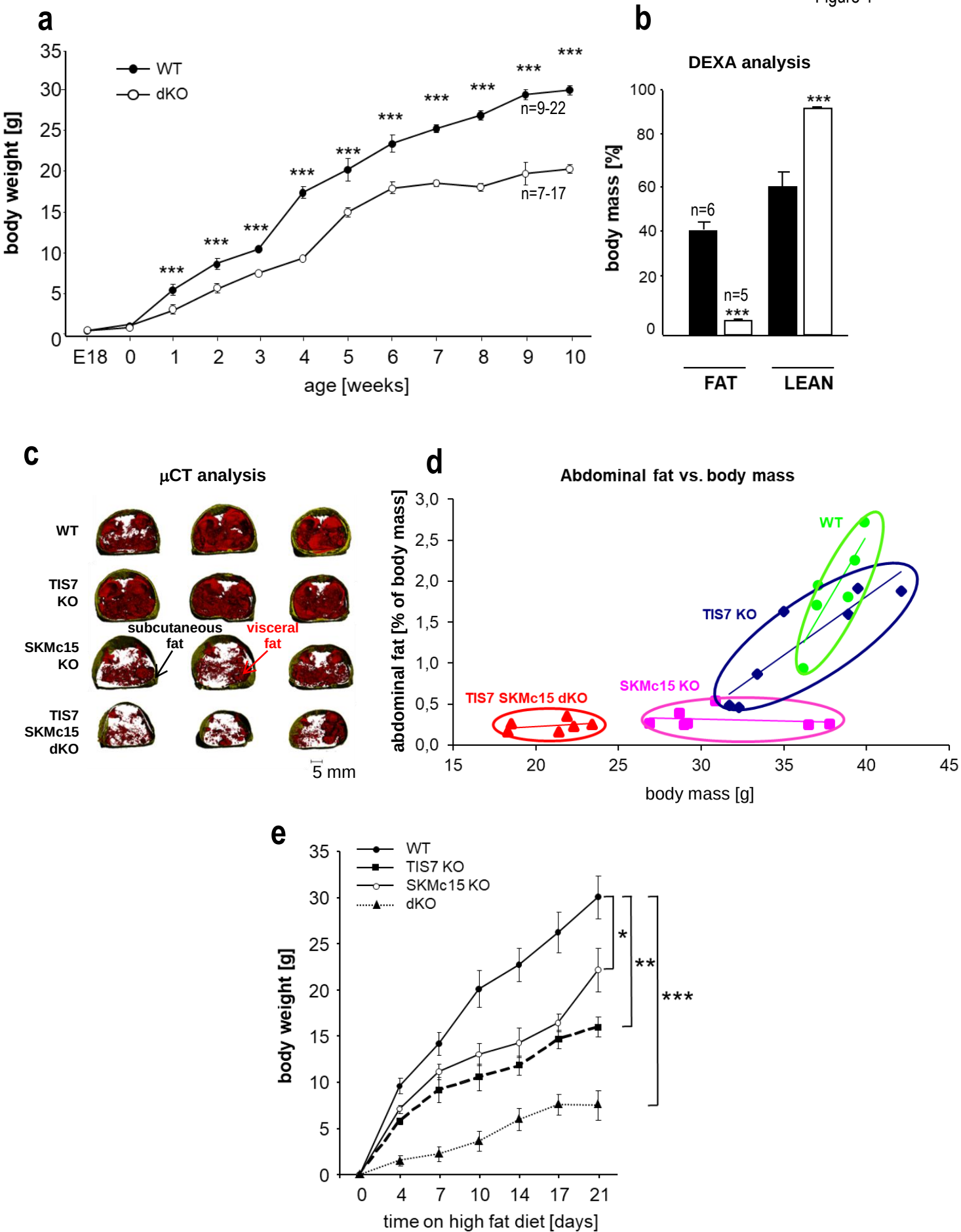

Figure 1. TIS7 SKMc15 dKO mice display postnatal growth retardation, less body fat and resistance against HFD-induced obesity.

a) Growth curves of WT (black circles) and TIS7 SKMc15 dKO (empty circles) male mice on chow diet. b) DEXA measurements of WT (black bar) and TIS7 SKMc15 dKO (empty bars) male mice. c) Micro-CT measurements mice identified a lack of abdominal fat in single and dKO mice. 3-dimensional reconstitution of images of the abdominal fat mass distribution in WT and KO mice. Yellow - subcutaneous fat mass, red - visceral fat mass. d) Mass contribution [%] of the abdominal fat in correlation to the total mass of the specimen [g]. A linear regression is overlaid for each group individually. The regression results for the WT group are y= 0,342x-11,13 with a R^2 of 0,74; for the TIS7 KO group y=0,143x-3,91 with a R^2 of 0,82; for the SKMc15 KO y=0,005x+0,48 with a R^2 of 0,04 and for the dKO y=0,011+0,01 with a R^2 of 0,1. ANCOVA analysis for the fat mass as a percentage of the body weigth as covariant was performed. e) Reduced gain of dKO mice body weight fed with HFD. Data shown are mean ± SEM, n≥9 per genotype, *P< 0.05, **P < 0.01, *** P < 0.001.

Figure 2

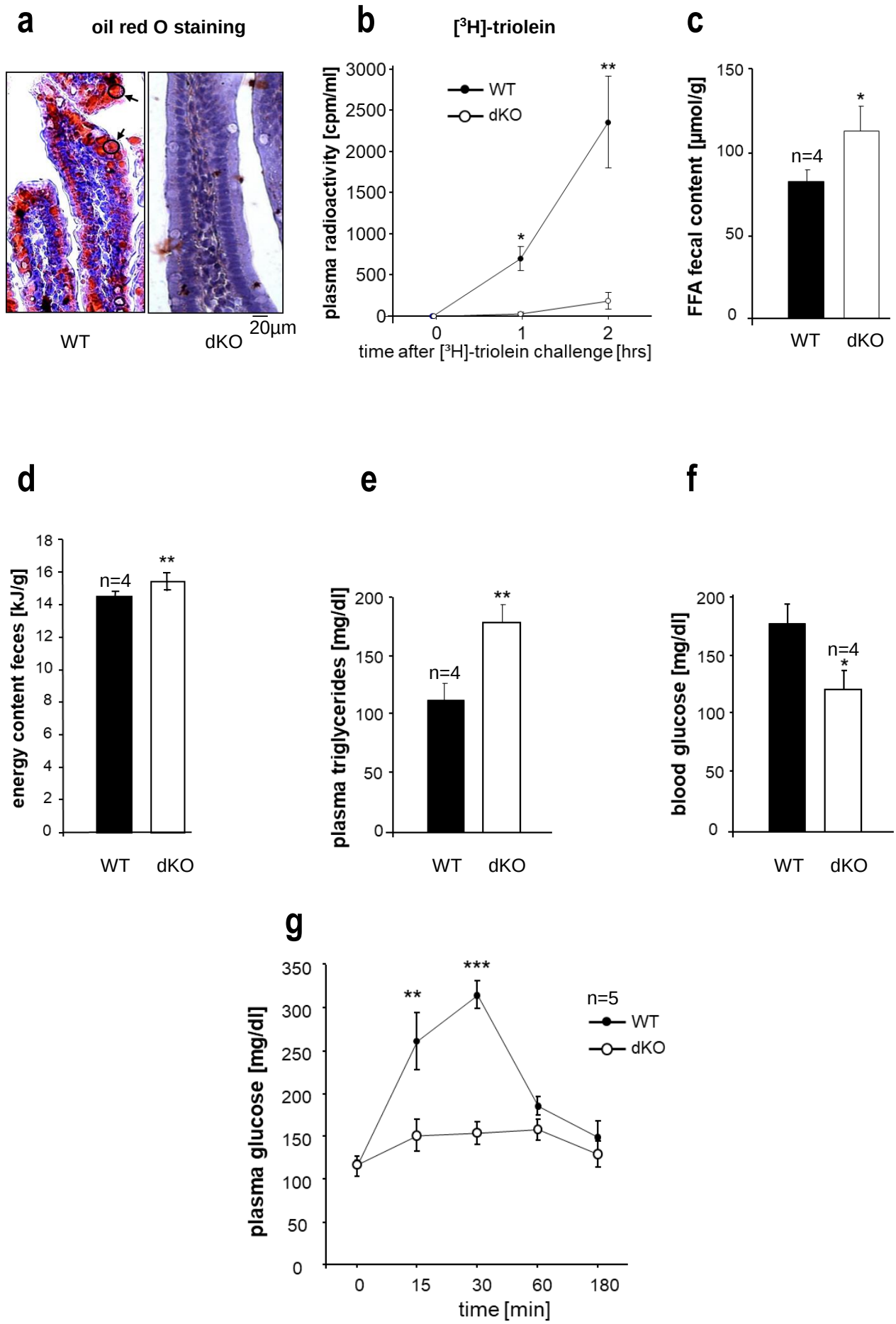

Figure 2. Fat uptake and metabolism are affected in TIS7 SKMc15 double knockout mice.

a) TGs accumulation in the intestines of mice 3 h after bolus oil feeding detected by oil red O staining. b) Radioactivity levels in plasma samples following [^{3}H]-triolein feeding, n=8, *P< 0.05, **P < 0.01. c) Concentrations of free fatty acids in the feces of mice fed with HFD, n=4, *P < 0.05. d) Energy content of dried feces samples determined by bomb calorimetry, **P < 0.01. e) TG levels in mice 4 hrs post olive oil gavage, **P < 0.01. f) Postprandial blood glucose levels, n=4, *P < 0.05. g) Glucose tolerance test, n=5, **P < 0.01, ***P < 0.001.

Figure 3

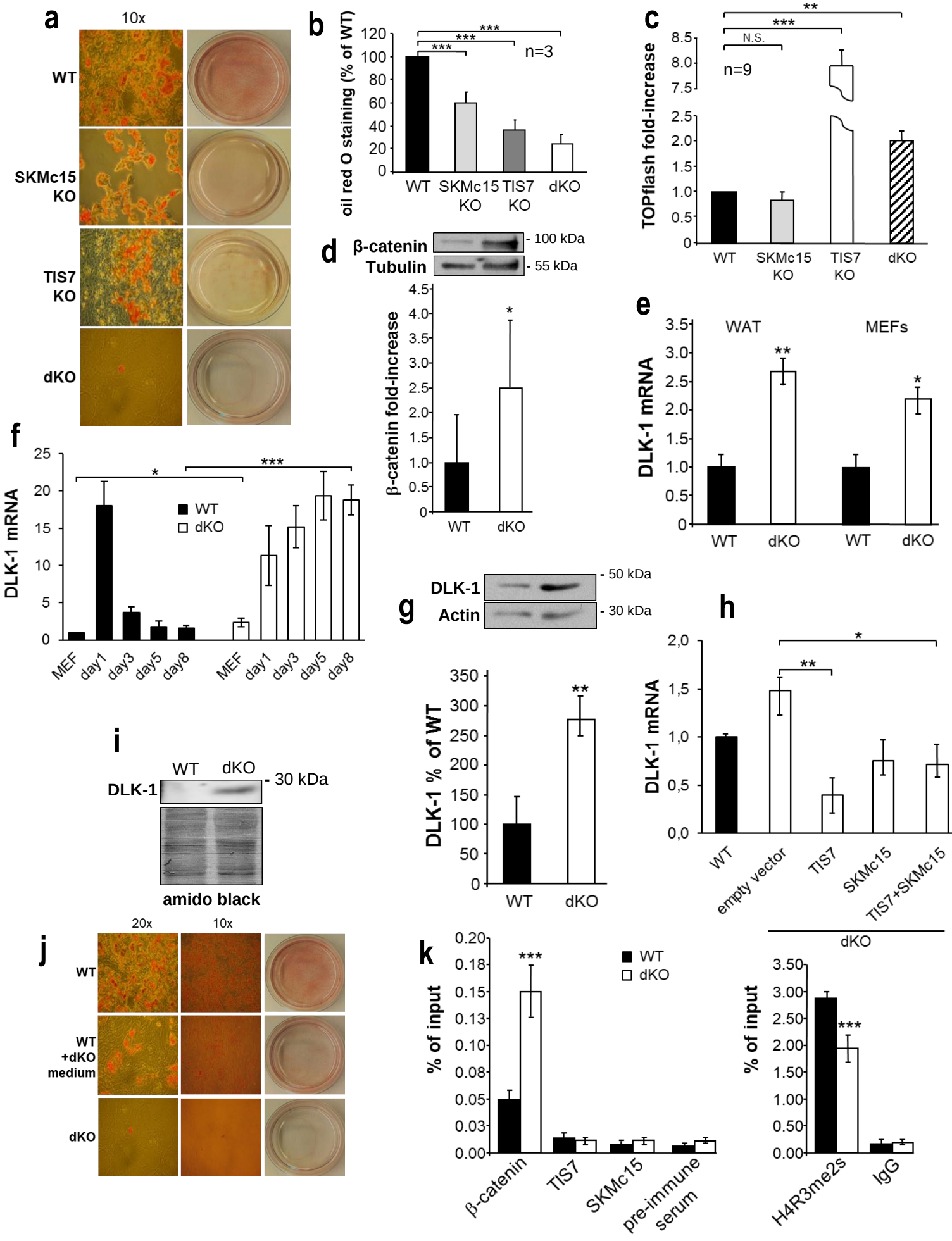

Figure 3. Adipocyte differentiation and Wnt signaling pathway are significantly affected in TIS7 SKMc15 dKO mice. a) Representative oil red O staining of MEF cells following 8 days of the adipocyte differentiation protocol. b) Quantification of oil red O staining from three independent adipocyte differentiation experiments. n=3; Student's t-test ***P<0.001. c) MEFs were transiently co-transfected with the pTOPflash luciferase reporter and β-galactosidase expression vectors. 48 h after the transfection luciferase and β-galactosidase activities were measured. Firefly luciferase activities were normalized on transfection efficiency using the β-galactosidase values. The experiment was repeated three times. Mean and standard deviations are shown. d) Western blot analysis of the total β-catenin amount in WT and dKO WATs. Quantification of 3 biological repeats; insert is one representative Western blot. Error bars indicate standard deviations. e) DLK-1 is significantly up regulated in TIS7 SKMc15 dKO mice. mRNA expression was measured by qPCR in WAT and MEFs. Values were normalized on GAPDH, n=3. Error bars indicate standard deviations. f) DLK-1 mRNA expression measured in MEFs treated with the adipocyte differentiation cocktail. WT MEFs values were set as 1. g) DLK-1 protein Western blot analysis in MEFs after 8 days of adipocyte differentiation cocktail treatment. Mean of 3 biological repeats; insert is one representative Western blot. h) DLK-1 in adipocyte-differentiating TIS7 SKMc15 dKO MEFs. WT MEFs values were set as 1, n=3; Student's t-test *P<0.05, **P<0.01. Error bars indicate standard deviations. i) TIS7 SKMc15 dKO MEFs secrete DLK-1 protein into the cell culture medium. Identical volumes of media from WT and dKO cells 8 days treated with the adipocyte differentiation cocktail were analyzed by Western blot using specific anti-DLK-1 protein antibodies. Equal loading of samples was evaluated by amido black staining of the membrane. j) TIS7 SKMc15 dKO MEFs-conditioned medium inhibited adipocyte differentiation in WT MEFs. MEFs were treated 8 days with the adipocyte differentiation cocktail. WT MEFs treated with the TIS7 SKMc15 dKO-conditioned medium showed reduced differentiation. k) ChIP analysis identified specific β-catenin binding to the DLK-1 regulatory element increased in TIS7 SKMc15 dKO samples. β-catenin, TIS7 and SKMc15 sera and histone H4R3me2s specific antibodies were used for the specific immunoprecipitations; pre-immune serum and IgG as background controls. Binding of β-catenin was significantly up and of symmetrically dimethylated histone H4 significantly down regulated in the 8 days differentiated TIS7 SKMc15 dKO MEFs. No significant difference was found in the binding TIS7 and SKMc15 proteins. n=3, error bars indicate the standard deviation, Student's t-test *P< 0.05, **P < 0.01, ***P < 0.001.

Figure 4

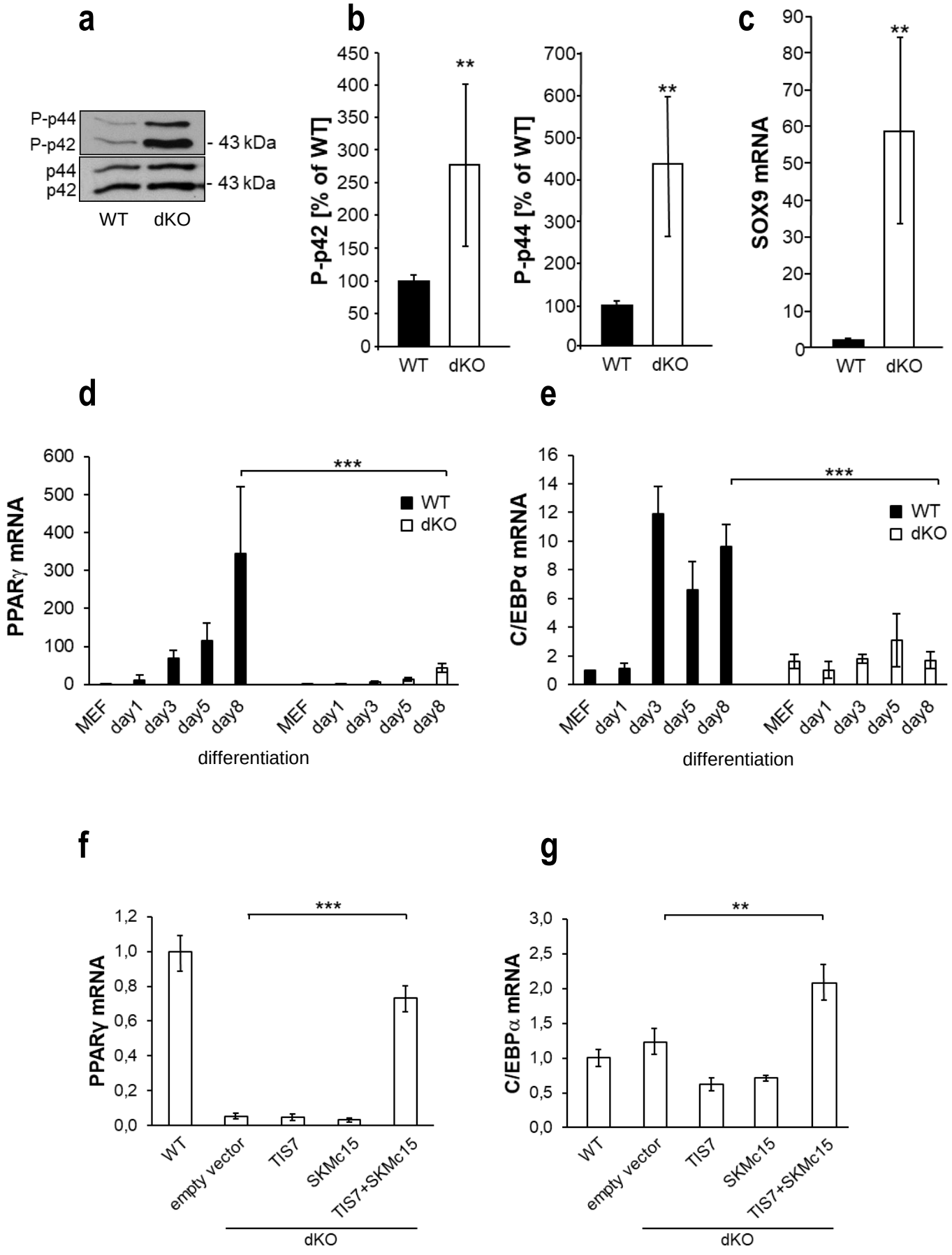

Figure 4. Adipocyte differentiation regulatory genes are down regulated and MEK/ERK pathway is up regulated in TIS7 SKMc15 dKO mice. a) Representative Western blots of phospho-p44 and phospho-p42 from 8 days adipocyte differentiation cocktail-treated MEFs. b) Normalization on p44 and p42; n=3. Error bars indicate standard deviations. WT values were set as 100 %. c) SOX9 mRNA levels were up regulated in TIS7 SKMc15 dKO MEFs. SOX9 expression was measured by qPCR in 8 days adipocyte-differentiated WT and dKO MEFs. SOX9 values were normalized on GADPH expression. WT MEFs values were set as 1, n=3. Error bars indicate standard deviations. Student's t-test **P < 0.01. d) PPARγ and e) C/EBPα mRNA levels were down regulated in TIS7 SKMc15 dKO adipocyte-differentiated MEFs. Gene expression was measured by qPCR and during 8 days treatment with the adipocyte differentiation cocktail. Values were normalized on GADPH expression. WT MEFs values were set as 1, n=3. Error bars indicate standard deviations. f) Ectopic co-expression of TIS7 and SKMc15 rescued levels of adipogenic genes PPARγ and g) C/EBPα. Student's t-test **P < 0.01, ***P < 0.001.

Figure 5

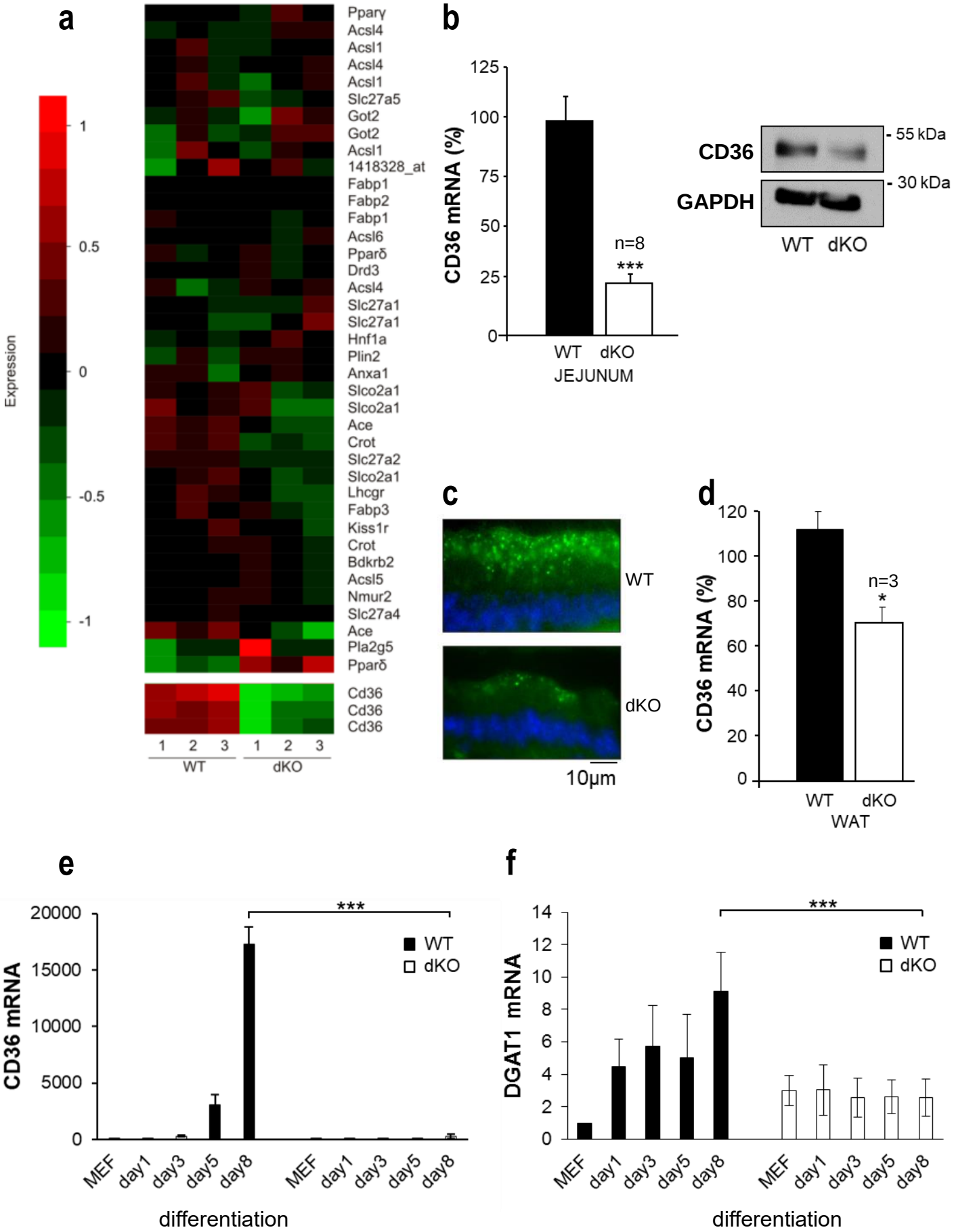

Figure 5. CD36 and DGAT1 levels are down regulated in TIS7SKMc15 dKO mice. a) Heatmap of hierarchical cluster analysis of intestinal genes' expression involved in lipid transport, altered in TIS7 SKMc15 dKO mice fed with HFD for 3 weeks. b) qPCR analyses of samples from jejunum of 3 weeks HFD-fed mice (qPCR mean ± SD; n=8) and a representative WB of jejunum protein lysate from WT and dKO mice. c) Jejunal sections of WT and TIS7 SKMc15 dKO mice fed with HFD, stained with anti-CD36 antibodies and with DAPI for documentation of nuclei (magnification 100x). d) qPCR analysis of CD36 mRNA levels in WAT, n=3. e) qPCR analysis of CD36 in MEFs differentiating into adipocytes. Relative expression levels were normalized on GAPDH expression. WT MEFs values were set as 1. f) DGAT1 mRNA levels were down regulated in TIS7 SKMc15 dKO adipocyte-differentiated MEFs. *P< 0.05, **P < 0.01, ***P < 0.001.

Figure 6

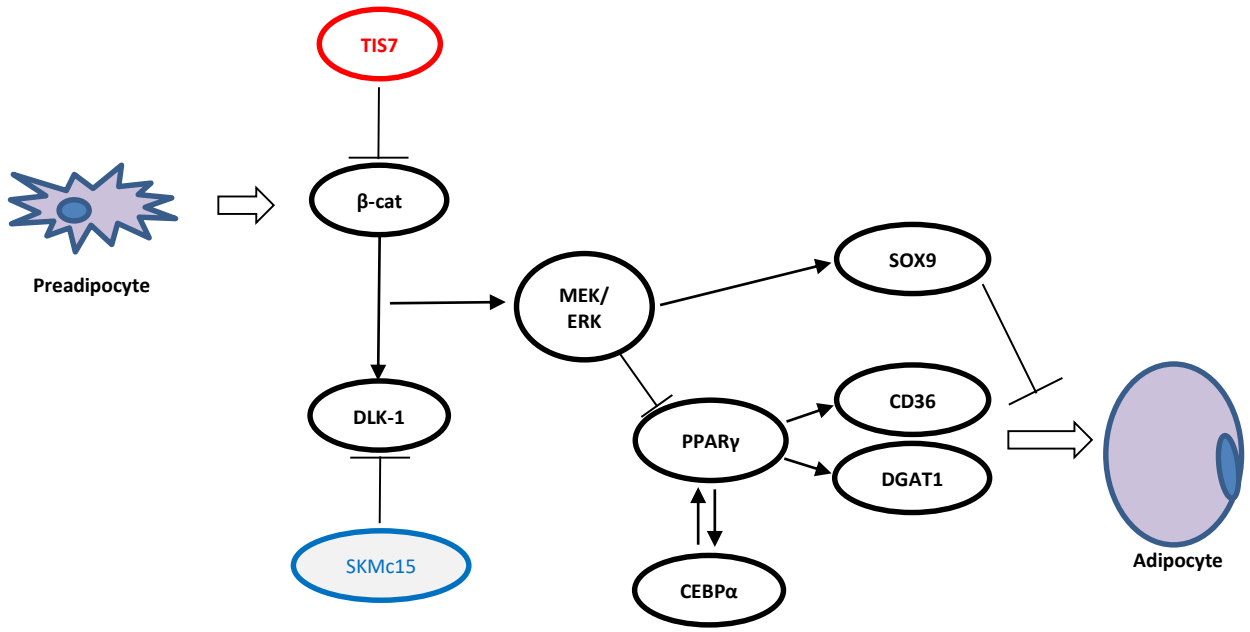

Figure 6. Proposed model of TIS7 and SKMc15 molecular mechanisms of action during adipocyte differentiation.

Supplementary figure 1

a

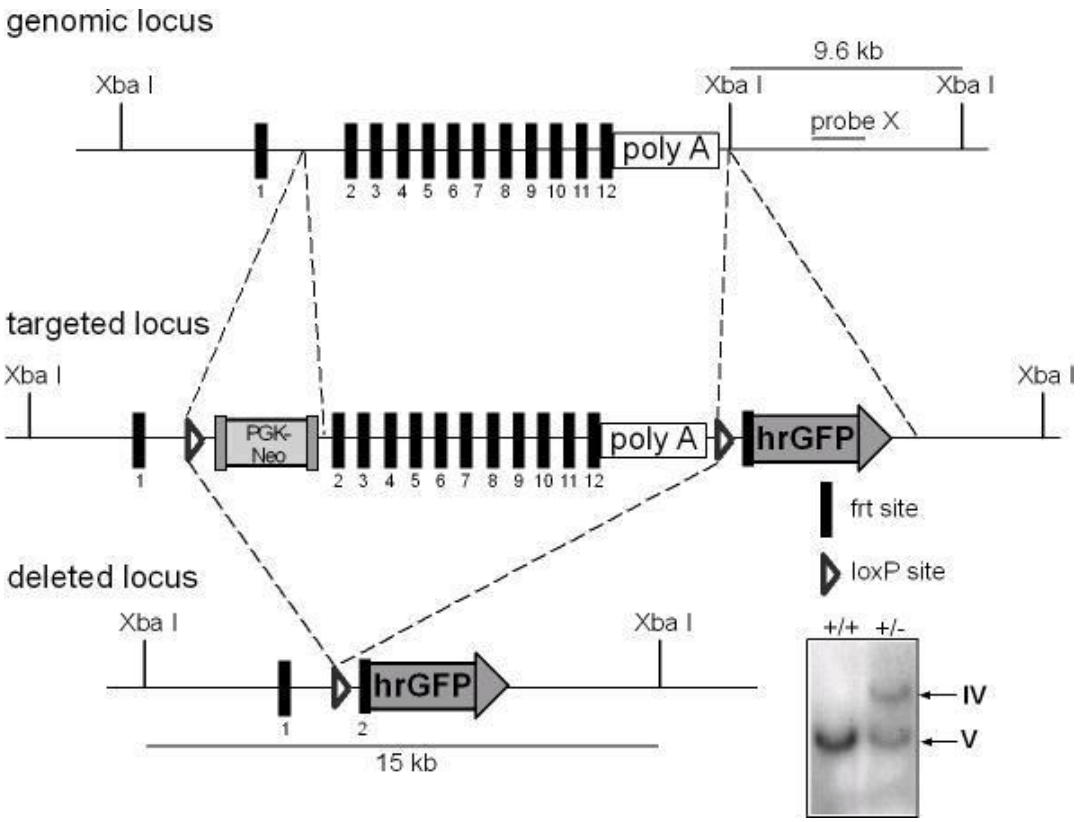

b

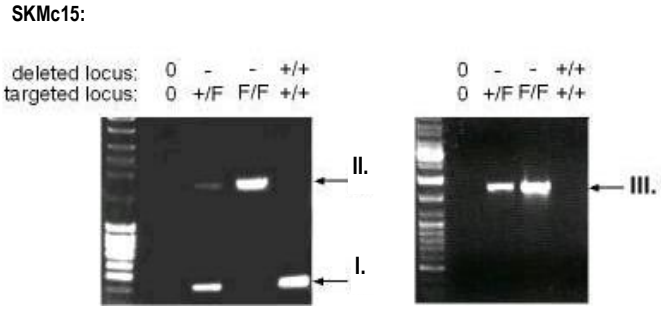

c

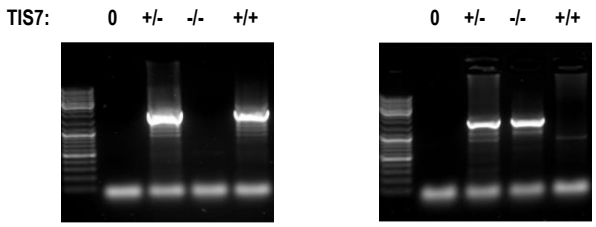

SKMc15 knockout

a) Southern blot analysis. The fragment detected by the Southern probe, was 9.6 kb in the wt (insert, band V) and 15 kb in the deleted locus (band IV). b) PCR genotype analysis of SKMc15 targeted and deleted alleles. **I**: 426 bp wt

SKMc15 PCR fragment. **II:** 1772 bp SKMc15 targeted allele PCR product. **III**: 1700 bp SKMc15 GFP screening PCR product can be amplified from the targeted (F) and the deleted allele (-/-), but not from the wt (+/+) locus. c) TIS7 PCR detection in TIS7 SKMc15 dKO mice. Left panel: detection of 1800 bp TIS7 wt allele; right panel: detection of 2100 bp TIS7 KO allele.

Supplementary figure 2

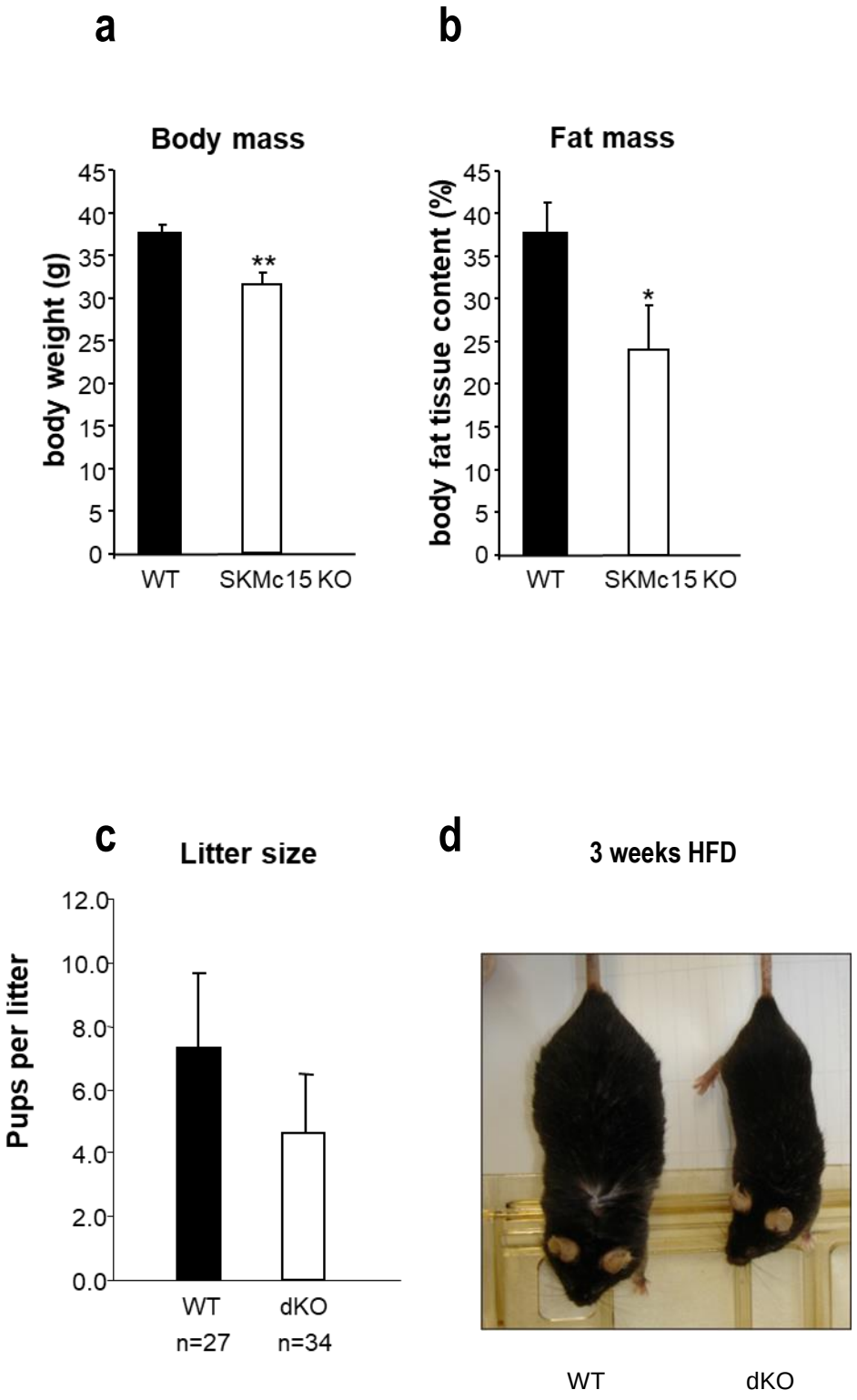

SKMc15 KO mice are smaller and have less fat than the WT controls. a) The total body weight of adult, sex- and age-matched SKMc15 mice was significantly smaller than their WT littermates. b) SKMc15 KO mice had significantly reduced fat mass when compared to their WT littermates. c) Significantly lower number of pups in TIS7 SKMc15 dKO mice ($P<0.01$) when compared to their WT littermates. d) Representative appearance of WT and TIS7 SKMc15 dKO male mice fed 3 weeks with HFD.

Supplementary figure 3

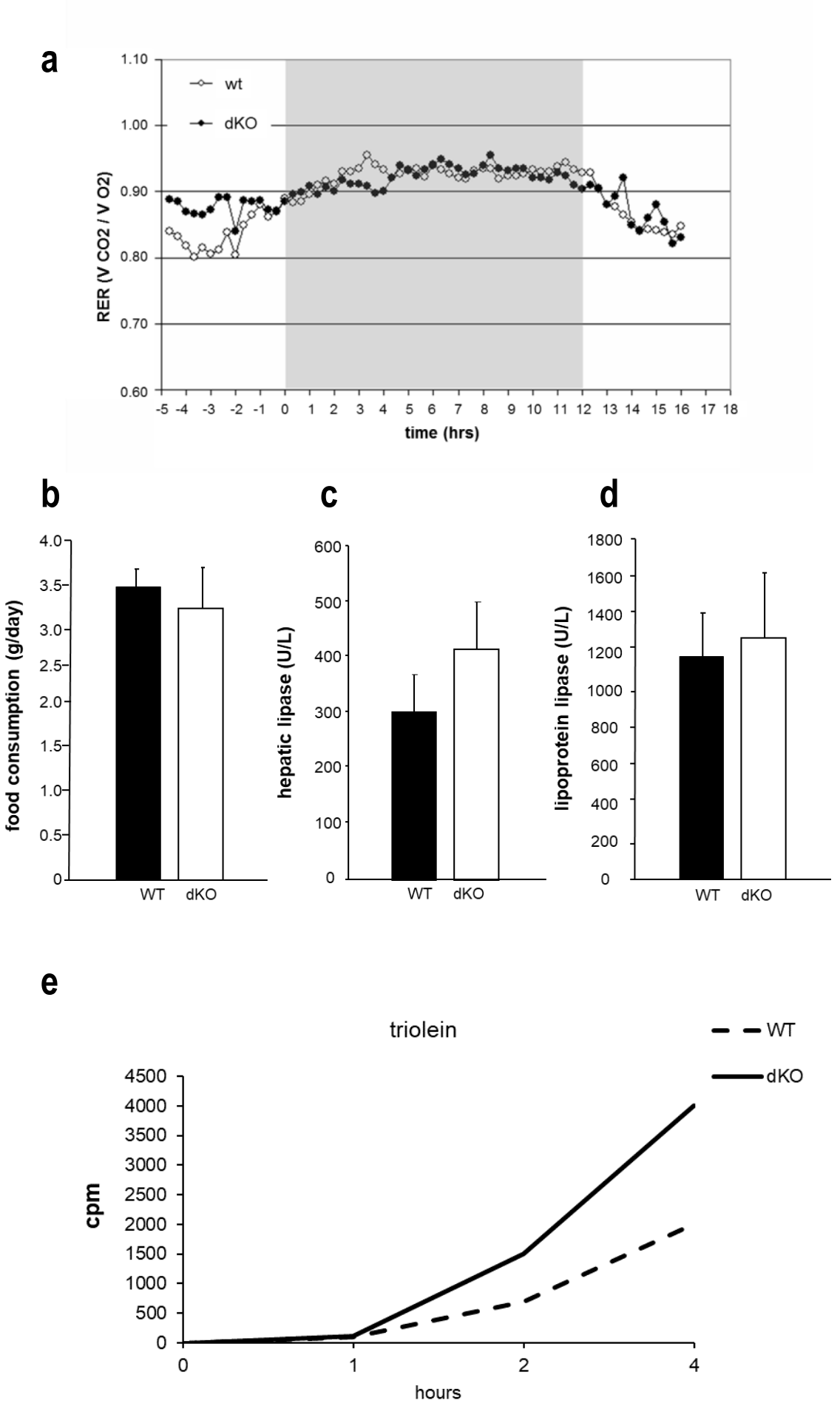

a) Respiratory exchange ratios (RER = VCO_2/VO_2) of WT and TIS7 SKMc15 dKO mice. No significant difference was observed apart from minor differences during the first hours of the trial b) No difference between WT and dKO mice in food consumption and levels of lipolytic enzymes following HFD feeding. HFD consumption of WT (n=4) and dKO (n=4) 8 weeks old male littermate mice. Data shown are mean ± STDEV. c) Hepatic lipase serum concentrations of WT (n=4) and dKO (n=4) 11 weeks old male mice after 3 weeks of HFD. d) Lipoprotein lipase serum concentrations of WT (n=4) and dKO (n=4) 8 weeks old male mice following 3 weeks of HFD e) Inability of TIS7 SKMc15 dKO mice to clear TGs from the circulation. Serum TG levels measured 4 hours after intragastric administration of olive oil.